J. Fluid Mech. (2010), *vol.* 644, *pp.* 281–319.
doi:10.1017/S0022112009992382

Concentration flux measurements in a polymer drag-reduced turbulent boundary layer

V. S. R. SOMANDEPALLI[1], Y. X. HOU[1]
AND M. G. MUNGAL[1,2]†

[1]Mechanical Engineering Department, Stanford University, Stanford, CA 94305-3032, USA
[2]School of Engineering, Santa Clara University, Santa Clara, CA 95053-0590, USA

(Received 2 October 2008; revised 20 September 2009; accepted 22 September 2009)

The drag-reducing action of dilute solutions of long-chain polymers in a flat-plate turbulent boundary layer is studied using particle imaging velocimetry (PIV) and planar laser induced fluorescence (PLIF). The results are used to characterize and quantify the spatial distribution of the injected polymer solution and the downstream development of the DR along the flat plate. The two techniques were used simultaneously to document and study the spread of the injected polymer solution and the resulting changes in the structure and statistics of the turbulence in the boundary layer. The PLIF images provide a qualitative and quantitative measure of the dispersion of the injected polymer solution. The mean and root mean square (r.m.s.) concentration profiles obtained using PLIF showed that the polymer greatly suppressed the turbulent dispersion in the near-wall region. The quantitative concentration measurements across the boundary layer, combined with simultaneous velocity measurements, are used to obtain concentration flux measurements in the boundary layer and are used to study the effect of the turbulence on the dispersion of the injected polymer. The variation of the fluxes with concentration of the injected polymer solutions and with increasing downstream distance is also studied and documented. The action of the polymer is to reduce the streamwise fluxes in the boundary layer, the suppression increasing with concentration. Further, the fluxes are also used to estimate the turbulent Schmidt number (Sc_T) for the drag-reduced flow. For the polymer injection experiments, the Sc_T are all greater than unity with the highest magnitude measured to be around 6, with the magnitude increasing with increasing concentration of the injected solutions. However, for each experiment, the estimated Sc_T decreases along the length of the flat plate reflecting the loss of polymer effectiveness.

1. Introduction

Drag reduction (DR) by polymer additives has been known for over 50 years (Toms 1948) and has been investigated ever since using experimental, analytical and computational means to understand the mechanics and the physics of this relatively complex phenomenon. The most outstanding feature is that one observes very significant reductions in the skin friction drag, up to 70 % in some cases, with the addition of very dilute solutions of high-molecular-weight polymer to turbulent flows. These concentrations are far below those that result in a significant increase

† Email address for correspondence: mungal@stanford.edu

in shear viscosity and therefore the DR effects are due to factors other than pure shearing forces. Key changes to the turbulent structure and flow statistics under the action of drag-reducing agents are at the heart of any DR mechanism. Therefore, it is instructive to investigate the phenomenon not only from a statistical approach, but also to consider the turbulent structures from a more descriptive point of view. A recent review of work performed to date on polymer DR is given by White & Mungal (2008).

The phenomenon of DR by polymer additives in turbulent flows was discovered and first reported by Toms in 1948. Virk *et al.* (1967) and Virk (1975) were the first to perform a comprehensive and exhaustive experimental investigation of the phenomenon in pipes and they were the first to demonstrate the existence of a maximum drag reduction (MDR) asymptote which was found to be independent of the polymer used and the pipe diameter. They also determined that the onset of DR occurs at a well-defined wall shear stress. Luchik & Tiederman (1988) used laser Doppler velocimetry (LDV) to measure velocity components in a drag-reduced channel flow and observed a dampening of the velocity fluctuations normal to the wall in the buffer region, an increased average time between bursts and an increase in the streak spacing. In a later work, Harder & Tiederman (1991) observed a reduction of Reynolds stress but the presence of the added polymer stress could only be accounted for at high concentrations of the polymer additive. Warholic, Massah & Hanratty (1999) observed approximately zero Reynolds stresses and a non-zero polymer stress over the whole cross-section of their channel. In a subsequent work, Warholic *et al.* (2001) confirmed the existence of a turbulent flow with zero Reynolds stresses across the entire channel at MDR with the use of particle imaging velocimetry (PIV). Walker & Tiederman (1990) investigated the DR produced by injection of polymer solutions at the wall in a channel flow.

Recognizing the importance of practical, external flow applications, several studies have concentrated on studying polymer DR in turbulent boundary layers (Wu & Tulin 1972; Fruman & Tulin 1976). Fontaine, Petrie & Brungart (1992) used LDV and laser-induced fluorescence to study the velocity field in a drag-reduced boundary layer with slot-injected polymer. They observed an immediate deceleration of the flow near the wall and a dramatic decrease of the wall-normal velocity fluctuations and Reynolds stress, due to action of the polymer. These effects relax substantially with increasing streamwise distance from the injection slot, becoming similar to the effects observed for dilute homogeneous polymer drag-reduced flows in channels. Petrie & Fontaine (1996) investigated and compared the effects of homogeneous drag-reducing polymer solutions and slot-injected polymer solutions in a boundary layer. While effects of homogeneous polymer solutions are noticeable across the entire boundary layer, the major effects of the injected polymer are restricted to the near-wall region. Despite these differences, modifications of the near-wall region and the amount of DR observed appear to be similar in both cases. These findings were confirmed by White, Somandepalli & Mungal (2004) who performed PIV measurements in a turbulent boundary layer with slot-injected polymer solutions. They found significant modifications of the near-wall structure of the turbulence with a coarsening of the low-speed streaks and a reduction in the number and intensity of the near-wall vortical structures. Using planar laser induced fluorescence (PLIF), Somandepalli, White & Mungal (2003) also demonstrated that the polymers tend to accumulate around the low-speed streaks in the near-wall region of the boundary layer.

White *et al.* (2006) also decomposed the friction drag into four dynamical contributions, following the approach of Fukagata, Iwamoto & Kasagi (2002). In

this way, they showed that DR is achieved by either, or both, an attenuation of the Reynolds stress and a reduction in the total stress gradient near the wall. Somandepalli, Hou & Mungal (2005) investigated the streamwise evolution of DR in a turbulent boundary layer and also observed the three distinct regions, i.e. the development, the steady state and the depletion of DR downstream of injection. In their experiments, when the polymer was injected into the flow at a higher local momentum thickness Reynolds number position, they observed that high drag reductions (HDRs) were maintained over a longer length of the flat plate suggesting that injection into a fully turbulent flow is beneficial in maintaining a longer steady-state DR region. Winkel *et al.* (2009) studied DR under very high Reynolds number conditions. In experiments performed in the William B Morgan Large Cavitation Tunnel facility, they were unable to reach and maintain MDR conditions. A transient MDR-like state was noted past the development region in their tests. Interested in real world applications where roughness would be present, Petrie *et al.* (2003) studied the effect of surface roughness on polymer DR in a turbulent boundary layer comparing both homogeneous polymer oceans and slot-injected polymer solutions. They observed that higher polymer concentrations are required as roughness increases in homogeneous polymer ocean flows. However, in the case of slot injections, the DRs obtained on rough surfaces are substantially larger than on a smooth plate.

According to Lumley (1969), who was among the first to propose an analytical mechanism for DR, the turbulence outside the viscous sublayer stretches the polymer chains at sufficiently large strain rates leading to a higher effective viscosity in the turbulent region and, therefore, to an increase in the thickness of the viscous sublayer, while the viscosity in the sublayer remains more or less that of the solvent since the polymer chains are not extended by the shear flow. DR is observed as a result of the decrease in the velocity gradient at the wall, thus reducing the shear stress at the wall. Tabor & de Gennes (1986) contested Lumley's explanation and argued that the polymers in turbulent flows exhibit elastic properties even at very low concentrations. Therefore they can store up some of the cascading energy of turbulence and this energy is not dissipated by viscosity thus giving rise to an effective DR. In light of this theory, the onset of DR and the MDR asymptote have been recently revisited by Sreenivasan & White (2000). Benzi *et al.* (2005) and Procaccia, Lvov & Benzi (2008) showed that the MDR asymptote is an edge solution of a turbulent boundary layer and any further DR beyond this asymptotic state would render the flow laminar. The authors were able to theoretically derive the log-law profile seen in HDR states and also explain the increased slope associated with the flow in these cases. Yoshizawa (2003) investigated the turbulence anisotropy for explaining the mechanism of DR, while L'vov *et al.* (2004) suggest a mechanism of DR by arguing that polymer stretching results in the suppression of momentum flux to the wall.

For realistic geometries and applications, experimental research, computations and models have been designed to study turbulent boundary layer flows. These experiments, while revealing, have not been sufficient to describe the development of a drag-reduced boundary layer. In particular, they have not been able to provide detail on the dispersion characteristics of the injected polymer solutions. The injected polymers actively interact with the turbulence and modify its structure and statistics but there is very little data available, at present, on how the polymers affect the turbulent fluxes close to the wall. The objective of the experiments presented in this paper is to characterize the spatial development and downstream evolution of DR due to injection of polymer solutions in a turbulent boundary layer. The drag-reduced boundary layer is probed at several locations along the flat plate using PIV and PLIF

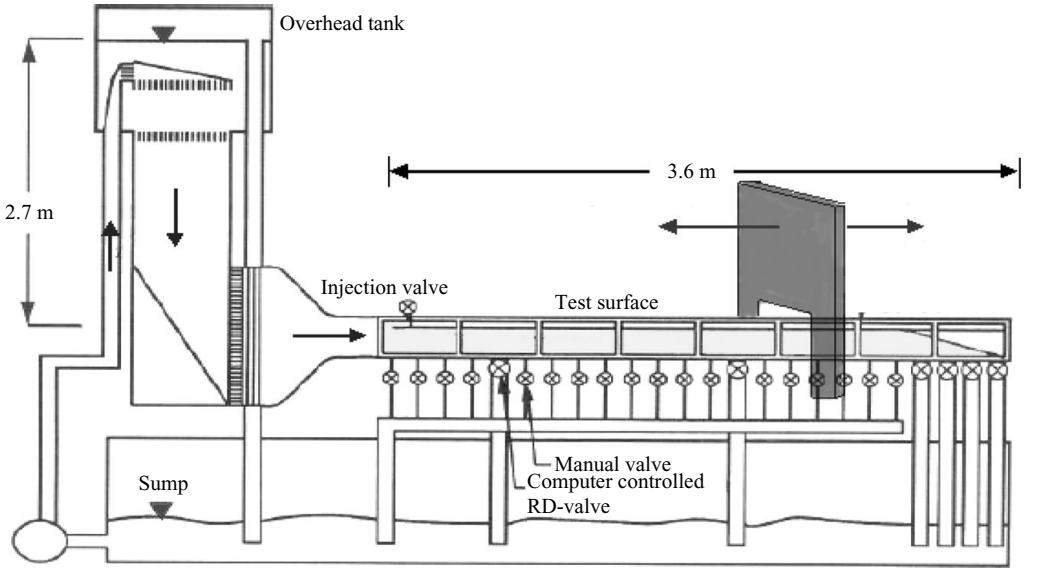

FIGURE 1. Schematic showing layout of the constant head closed circuit water tunnel facility.

to study the state of the flow. PLIF, of dye mixed with the polymer, is used to study the concentration, spread and dispersion of the injected polymer. Both PIV and PLIF measurements are made simultaneously and this allows the velocity data from PIV to be combined with the concentration data from PLIF. Using this technique, turbulent concentration fluxes can be calculated for drag-reduced flow for the first time. The PIV results obtained in these experiments represent a subset of a more comprehensive set which have been presented and analysed in detail in Hou, Somandepalli & Mungal (2008) and, as such, they are only presented in this paper very briefly to enable readers to be able to relate the concentration and concentration flux measurements, and for completeness. The experimental results presented here can be used to benchmark and fine tune numerical simulations, which are being developed to study and apply the phenomenon of DR to flows in practical applications.

2. Experimental

The experiments were conducted in a constant head closed circuit water tunnel, shown schematically in figure 1. The test section has a cross-section of 0.36 m in span and 0.13 m in height with a length of 3.66 m. The top and side walls of the test section are constructed of Plexiglas to provide full optical access to the flow and for mechanical access. The boundary layer test surface is the upper wall of the test section. Just upstream of the test surface is the leading edge plate on which the fresh boundary layers are started. A critical feature of the stainless-steel leading edge is its shape: a half-elliptical nose with a major to minor axis ratio of 16:1. Two boundary layer trips were used to ensure that the developing boundary layer was fully tripped to the turbulent state. The bottom wall and the side walls of the tunnel have slots built into them which are used to bleed the boundary layers that grow on these walls to control the free-stream velocity gradient. A detailed description of the experimental facility is given in Somandepalli (2006). To ensure that the polymer solutions used for the experiments were injected into turbulent flow, a slot 0.45 mm wide, inclined at

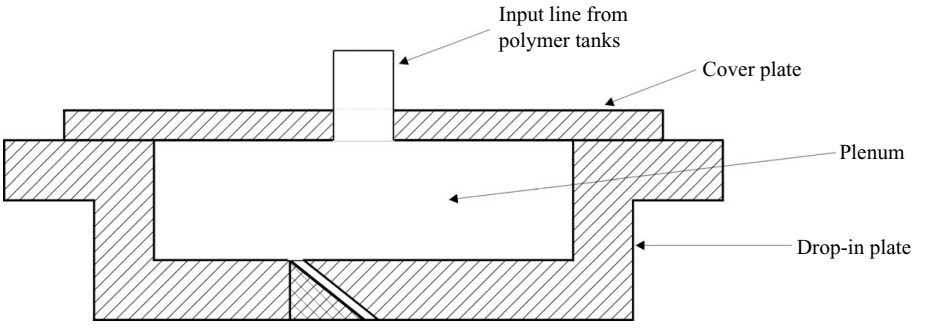

FIGURE 2. Side view schematic of composite injection slot assembly used for polymer DR experiments.

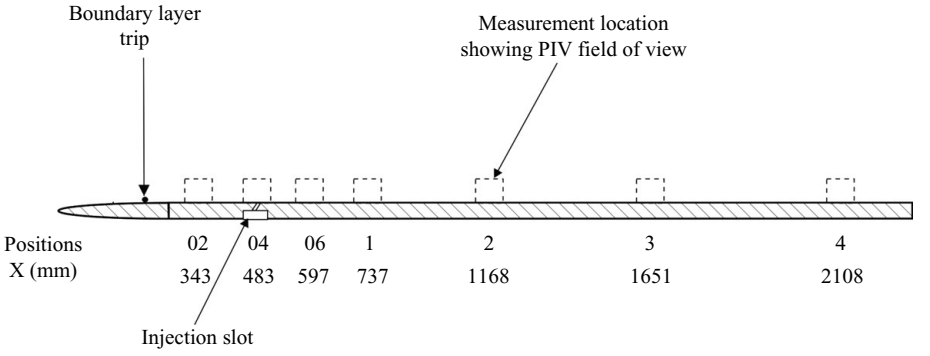

FIGURE 3. Schematic showing boundary layer flat plate, measurement locations and their distances (not to scale).

30° to the injection surface was cut downstream of the boundary layer trips to form the slot through which the polymer solution was injected into the boundary layer. A side view schematic of the composite injection slot is shown in figure 2.

Five downstream measurement stations are located along the length of the plate where data required to study the streamwise development of the boundary layer can be obtained. The first two measurement locations are closely spaced to the leading edge to clearly study this region, where growth of the boundary layer is the most critical, and the last three measurement locations were used to give an overall understanding of the flow development along the length of the tunnel. A schematic of the flat plate is shown in figure 3 with the measurement locations marked. The measurement locations on the flat plate are labelled positions 06 and 1, 2, 3 and 4 in order of increasing downstream distance. The injection slot described above was positioned at a port on the test surface which was located at position 04. The flow immediately downstream of injection is measured at position 06. Measurements upstream of the injection slot were made to characterize the boundary layer ahead of the injection slot and this location is labelled as position 02. For the experiments presented here, the tunnel was run at a constant free-stream velocity of 0.5 m s^{-1}. At this velocity, the flow is turbulent at all the measurement stations on the flat plate. Table 1 gives a summary of the distance of each of the measurement locations from the leading edge and the Newtonian boundary layer parameters for a free stream velocity of

Typical boundary layer parameters at measurement locations	X (mm) (X^+)	δ (mm) (δ^+)	θ (mm)	Re_θ
Position 02	343	13	1.56	700
Injection slot	483	16	1.8	840
Position 06	597 (12 500)	18 (376)	2.19	990
Position 1	737 (15 400)	20 (420)	2.54	1150
Position 2	1168 (24 000)	27 (565)	3.43	1550
Position 3	1651 (31 500)	35 (730)	4.47	2030
Position 4	2108 (40 200)	42 (900)	5.26	2380

TABLE 1. Typical boundary layer parameters at measurement locations; free stream velocity $= 0.5$ m s^{-1}.

0.5 m s^{-1}. The boundary layer parameters, both in physical units and normalized by the local friction velocity at each location, are also shown in this table.

The polymer used in the DR experiments is Poly-ethylene oxide (PEO), brand name POLYOX (tm) WSR-301 from Dow Chemical Co. This polymer, in powder form, has a mean molecular weight of about 4.5 million with a polydispersity (ratio of number average molecular weight to weight average molecular weight) of 1.45. Solutions of this polymer were prepared by directly mixing the polymer powder with water. The DR obtained in the water tunnel was varied by varying the concentration of the injected polymer solution.

2.1. *Flow diagnostics*

PIV was used to measure velocity and velocity statistics in these experiments. The PIV system used a Peltier cooled 12 bit CCD camera with a resolution of 1280×1024 pixels, a dual head – pulsed Nd:YAG laser operating at 532 nm, and appropriate sheet forming optics. A 532 nm narrow band filter was used in conjunction with the camera optics to allow only the laser light scattered by the tracer particles into the camera. The flow was naturally seeded with residual dust particles in the water of size less than 10 microns. All particles above this size were removed by a series of filters before the water entered the tunnel system. The natural seeding by dust in the water gave consistent and good particle images and hence all PIV measurements were performed with this. One thousand image pairs were acquired at each streamwise location and averaged to give the velocity profiles and statistics. A detailed and complete description of the PIV system and the algorithms used is presented in Hou *et al.* (2008) and Somandepalli (2006).

PLIF was used to quantitatively measure the concentrations of the injected polymer solution in the boundary layer. The PLIF measurement system was piggybacked on the existing PIV set-up to simplify the optics and also to ensure high quality of the data obtained. Rhodamine-WT, used in the experiments presented here, fluoresces under the action of 532 nm light (Putorti, Everest & Atreya 2003) and the emitted light used for concentration measurements is well separated from the excitation wavelength. A Schott glass filter, OG-550, from CVI Laser Inc., was used to filter out the laser excitation light in these experiments. The emitted light was captured using a second CCD camera of the same type as the one used for the PIV system.

2.2. *Combined PIV and PLIF measurements*

The PLIF camera was situated on the opposite side of the tunnel with respect to the PIV camera, figure 4. As a result, the region imaged by the PLIF camera was

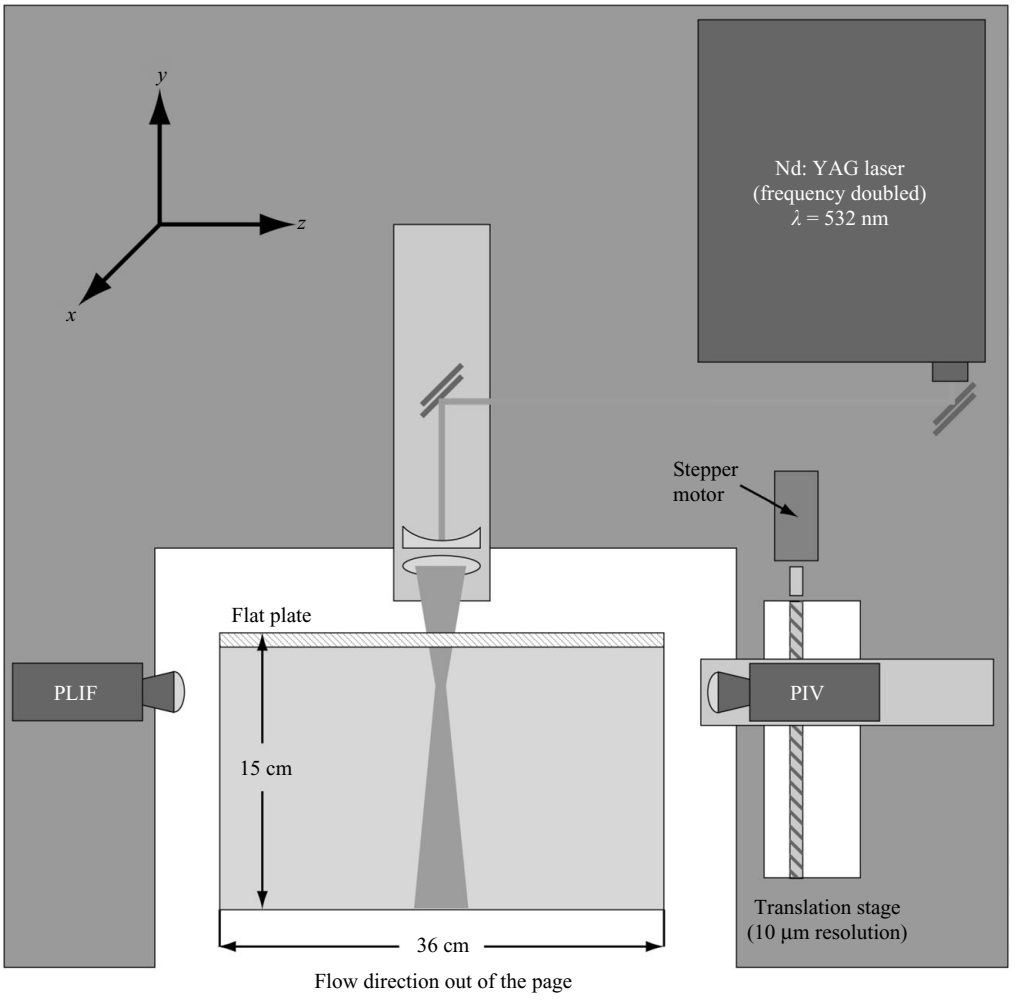

FIGURE 4. Schematic of optical breadboard showing cameras, laser and instrumentation layout.

laterally inverted compared to the image from the PIV image. The cameras were situated such that the regions imaged by each camera had the maximum overlap with the other. The PLIF camera lens was operated at a slightly lower magnification than the PIV lens (PLIF image size: PIV image size $= 1.04 : 1$) so that the PLIF camera saw a slightly larger field of view and completely enclosed the region seen by the PIV camera. The PLIF image was corrected for linear, rotational and angular distortions using standard image processing and rotation algorithms. Appropriate scaling for the PLIF images with respect to the PIV images was calculated and used in all experiments to match individual vectors with the polymer concentration at their respective locations on each image.

As part of the PIV measurements, 1000 image pairs are obtained at each measurement location in every experiment. Correspondingly, 1000 PLIF images are also simultaneously obtained. The PIV vectors are processed to obtain fluctuating velocity vector frames by subtracting the mean velocity profiles from each raw velocity vector frame. Each of these fluctuation velocity vector frames consists of a 64×80

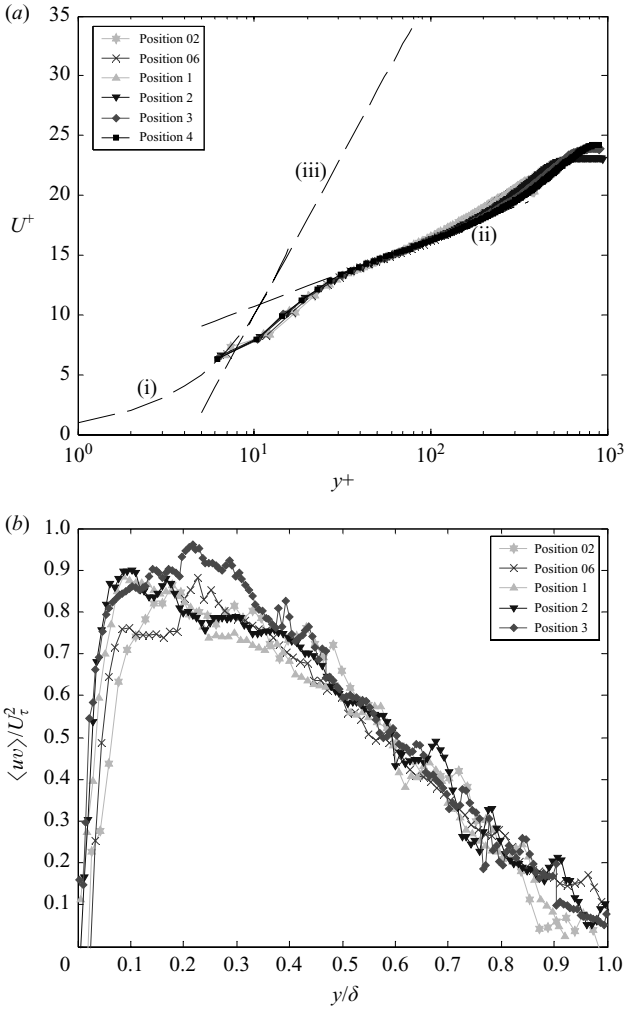

FIGURE 5. Measured velocity profiles in the water tunnel facility. (*a*) Mean velocity profiles in inner coordinates and (*b*) Reynolds stress profiles. Also shown in (*a*) are (i) $u^+ = y^+$ line, (ii) theoretical log law for a Newtonian turbulent boundary layer profile and (iii) MDR asymptote.

array of velocity vectors. The PLIF images are processed to extract the concentration of the injected polymer at the location of every PIV vector. An average polymer concentration at this location is calculated by binning a square region of size 15×15 pixels around the location of the PIV vector to obtain an average value of the polymer concentration at this location. This algorithm is executed for each of the 64×80 vectors in each PIV vector frame to give a frame containing 64×80 values of the polymer concentration for each PLIF image.

3. Measurements

3.1. *Baseline Newtonian flow*

For each run condition, PIV and PLIF measurements are made at all measurement stations in a purely Newtonian flow with no injection. This provides a baseline case against which the polymer injection case can be compared. Figure 5(*a*) shows the mean

velocity profile, in inner coordinates, obtained with no injection at all measurement locations. Also shown on the same graph are the lines showing (i) the $U^+ = y^+$ line, (ii) the theoretical log law for a turbulent boundary layer velocity profile and (iii) the MDR asymptote. The log law for a turbulent boundary layer velocity profile is described as

$$U^+ = 2.44^* \ln y^+ + 5.1, \tag{3.1}$$

while the MDR asymptote is given by the following equation as presented in Virk (1975) and Benzi *et al.* (2005):

$$U^+ = 11.7^* \ln y^+ - 17.0, \tag{3.2}$$

where U^+ and y^+ are the velocity and distance from the wall scaled in wall units. The measured mean profiles, at each location, are in good agreement with the theoretical mean profile at these measurement locations. Figure 5(*b*) shows the Reynolds stress profiles at these locations obtained from the PIV data. The profiles show that the quality of the boundary layer is uniform along the length of the tunnel.

To quantify the effect of the injection process on the boundary layer, an experiment was performed where water was injected through the injection slot at the same conditions that were used for polymer injection experiments. The mean velocity profiles obtained for this case are shown in figure 6(*a*). As can be seen from the graph, the injection of water into the boundary layer has no discernible effect on the mean velocity profiles measured downstream of injection. All the measured mean velocity profiles collapse on the theoretical log-law profile for a Newtonian boundary layer. Figure 6(*b*) shows the comparison of the Reynolds stress profiles measured at positions 06, 1 and 4 on the flat plate for the Newtonian and the water injection cases. The open symbols represent the Newtonian case and the solid symbols represent the measurements from the water injection case. The very negligible changes in the shear stress measured at all locations on the flat plate indicate that the injection system does not affect the Newtonian boundary layer in any significant way. This conclusion is critical since it rules out the possibility of the injection system contributing to the drag changes as measured in the polymer injection experiments.

Figure 7 shows the PLIF images obtained for the case of water injection. The images are arranged in order of increasing downstream distance starting with position 06. At position 06, (figure 7*a*) the measurement position closest to the injection slot, the injected fluid is dispersed through about 50 % of the boundary layer by the action of the turbulence in the mean flow. The large-scale swirling nature of the turbulent flow is also clearly seen in the image. The dark regions in the images are regions where there is no injected dye present and these are interspersed with the regions where the fluorescent dye in the injected liquid is present showing vigorous mixing by the turbulence. Further downstream, with increasing distance, the injected dye solution is mixed into the mean flow by the action of the turbulence. The flow, at downstream locations, does not show much large-scale swirling motions with sharp gradients in the fluorescence signal. However, this does not imply that such motions are absent, but just that they cannot be revealed by a relatively uniform and well-mixed dye concentration.

3.2. *Polymer injection experiments*

Figures 8–10 show (*a*) the mean velocity profiles and (*b*) the Reynolds stress profiles, obtained in the experiments with 100 ppmw (part per million by weight), 250 ppmw and 500 ppmw polymer solution injection. The mean velocity profiles are plotted in inner coordinates while the local friction velocity at each measurement location is used to normalize the Reynolds stress profile at that location. In the 100 ppmw

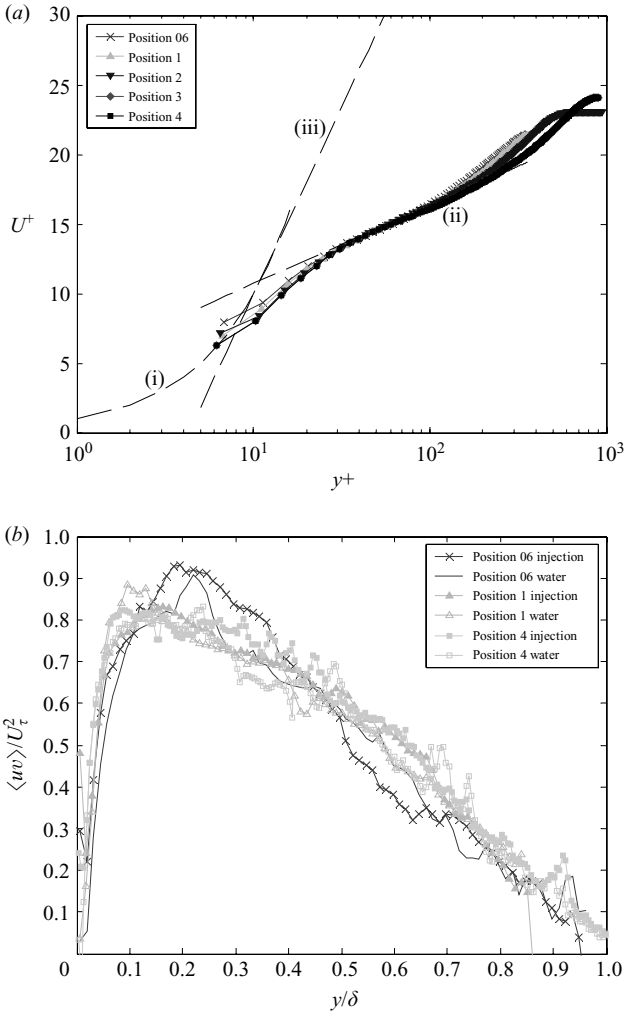

FIGURE 6. Comparison of velocity profiles showing effect of injection slot: (*a*) mean velocity profiles in inner coordinates and (*b*) Reynolds stress profiles. Also shown in (*a*) are (i) $u^+ = y^+$ line, (ii) theoretical log law for a Newtonian turbulent boundary layer profile and (iii) MDR asymptote.

case (figure 8), the DR obtained at position 06 is about 35 % which increases to 45 % at position 1. Downstream of this position, the DR due to the injected polymer decreases as the polymer is mixed into the outer regions of the boundary layer by turbulent dispersion and loses its effectiveness. At position 4, the last measurement position, the directly measured DR increases from the previous position to about 15 %. This increase in the DR from position 3 to position 4 is attributed to the buildup of the injected polymer in the tunnel system. This measurement location is the last one that was probed and the background homogeneous concentration of the polymer in the tunnel rises to about 0.7 ppmw which is sufficient to show a small DR in the flow (Warholic *et al.* 1999). Figure 8(*b*) shows the Reynolds shear stress profiles, normalized by the boundary layer thickness and the local shear velocity, obtained for the same case. The Newtonian reference case is shown as a solid line and the

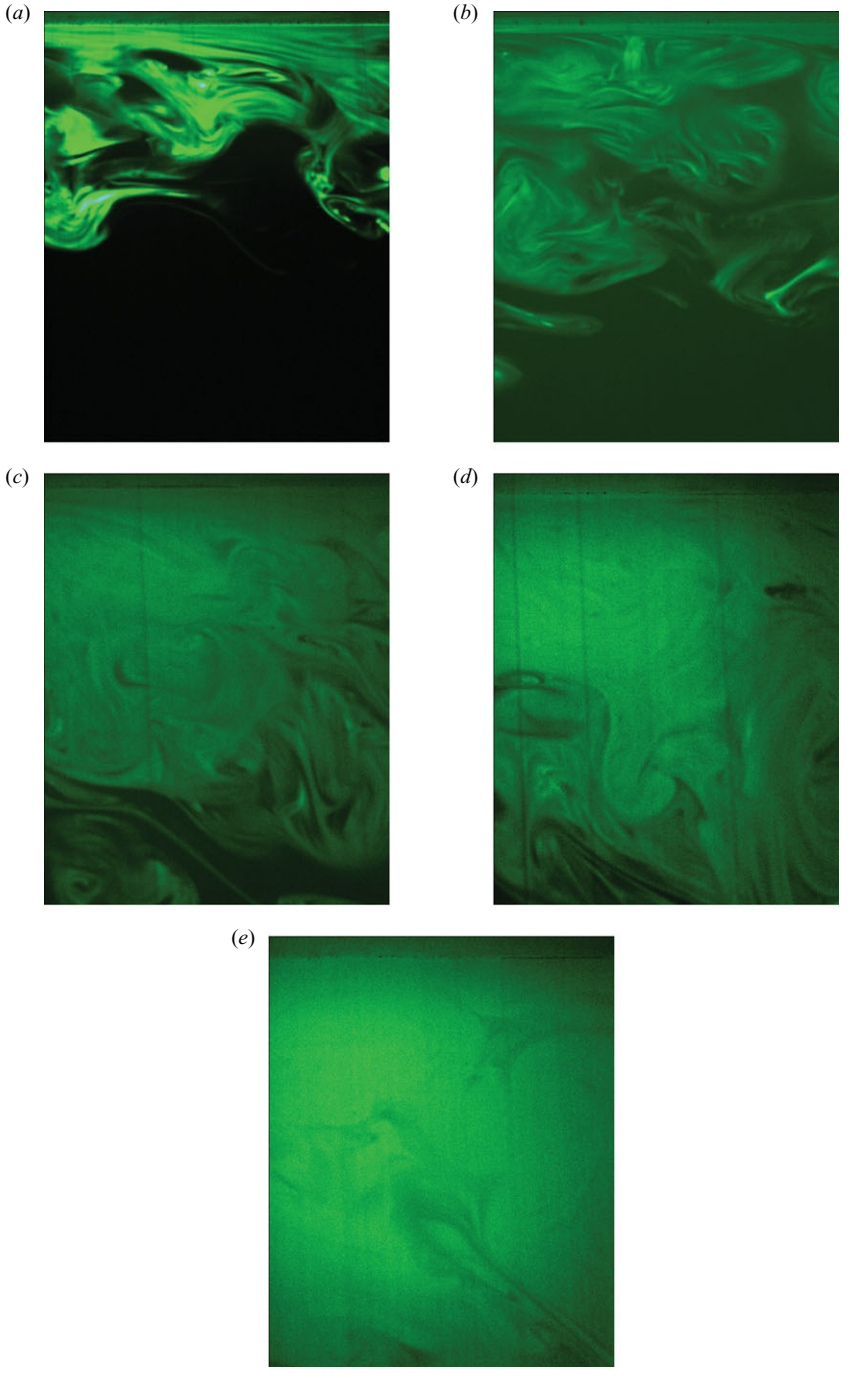

FIGURE 7. Typical PLIF images observed for the case of water injection. Images obtained: (*a*) at position 06, (*b*) at position 1, (*c*) at position 2, (*d*) at position 3 and (*e*) at position 4. In each case, image size is 17.5 mm $\times$ 14.3 mm (H $\times$ W).

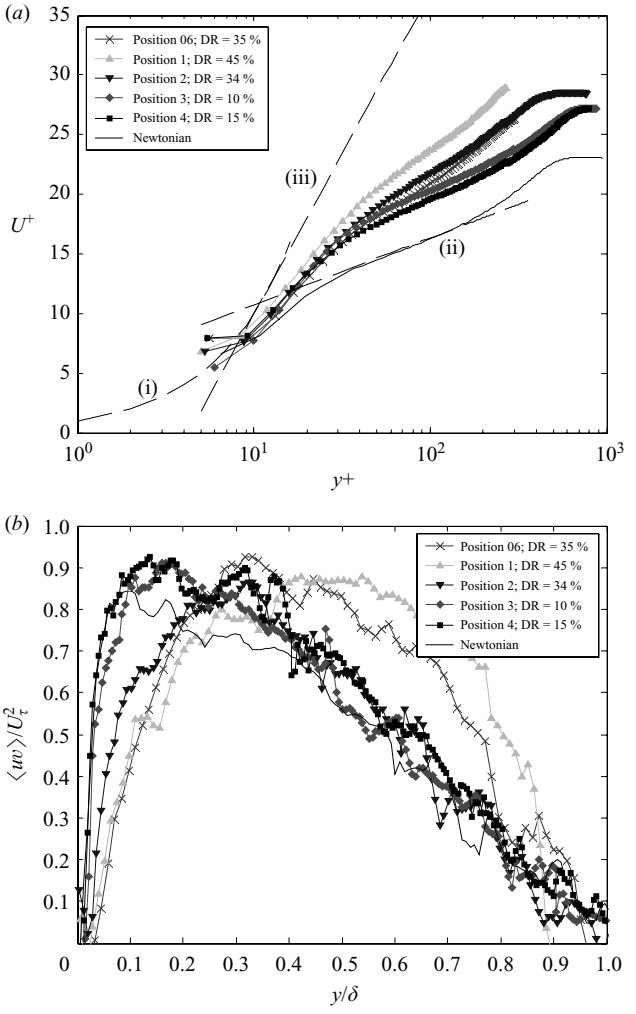

FIGURE 8. Velocity profiles for the 100 ppm polymer solution injection case. (*a*) Mean velocity profiles obtained at each measurement location shown along with (i) $u^+ = y^+$ line, (ii) theoretical log law for a Newtonian turbulent boundary layer velocity profile and (iii) MDR asymptote. (*b*) Reynolds stress profiles obtained at each measurement location compared to Newtonian Reynolds stress profile.

measured Reynolds stresses at each location are marked by the symbols as given in the legend. At positions 06, 1 and 2, the polymer injection reduces the Reynolds stress measured close to the wall ($y/\delta < 0.3$). Further downstream, at positions 3 and 4, the polymer has little effect on the normalized Reynolds stress profile which remains similar to the Newtonian Reynolds stress profile.

The mean velocity profiles obtained from the injection of a 250 ppmw concentration solution of the polymer are shown in figure 9(*a*). The 250 ppmw solution gives higher DRs along the entire length of the boundary layer compared to the 100 ppmw solution described above. An important feature to notice in the mean velocity profiles with DRs greater than 40 % is the change in the slope of the log-law region of the profile. The slope of the log law increases after about 40 % DR and this regime is typically referred to as the high drag reduction (HDR) regime in the literature. DRs lower than

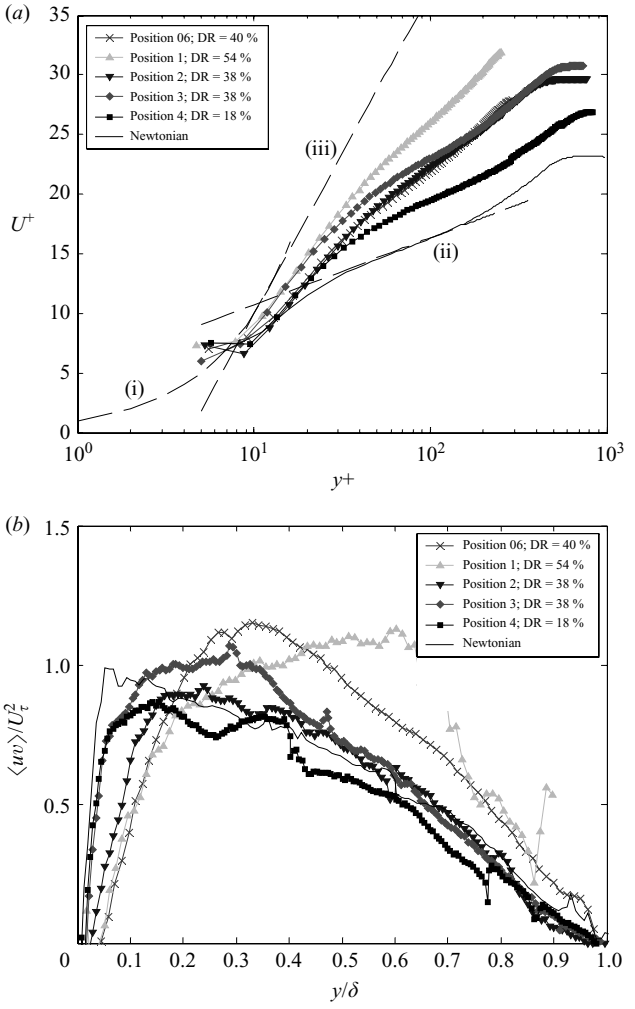

FIGURE 9. Velocity profiles for the 250 ppm polymer solution injection case. (*a*) Mean velocity profiles obtained at each measurement location shown along with (i) $u^+ = y^+$ line, (ii) theoretical log law for a Newtonian turbulent boundary layer velocity profile and (iii) MDR asymptote. (*b*) Reynolds stress profiles obtained at each measurement location compared to Newtonian Reynolds stress profile.

40 % fall in the low drag reduction (LDR) regime and they are characterized by the upward shift of the log-law region with its slope remaining constant. In the case of the 250 ppmw polymer concentration injection experiment, positions 06 and 1 show HDR-like behaviour and the positions further downstream all fall in the LDR regime. Figure 9(*b*) shows the corresponding Reynolds stress profiles. At positions 06 and 1, the Reynolds stress in the near-wall region is drastically suppressed by the action of the polymer close to the wall. This is evident from the rapid decay of the Reynolds stress profiles at these locations for values of $y/\delta < 0.3$. The inner regions of the mean velocity profiles (the buffer layer and the sublayer) show a slight deviation from the Newtonian profile at positions 06 and 1. Similar deviations have also been observed by Fontaine *et al.* (1992) at equivalent measurement locations. In their experiments, they observed a deficit in the mean velocity profiles measured at $x^+ = 9200$ and 22 600.

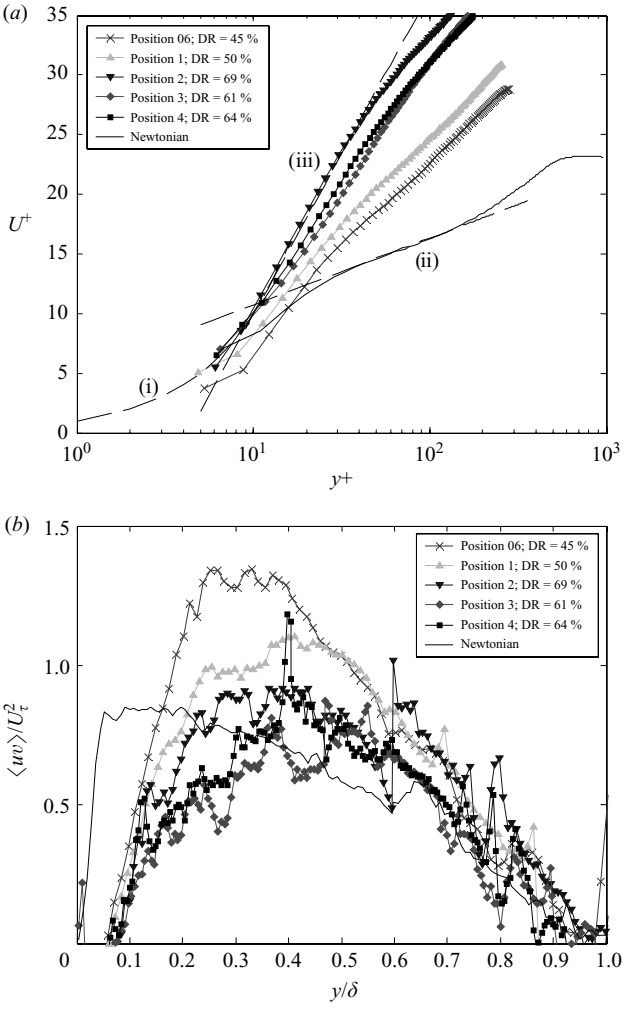

FIGURE 10. Velocity profiles for the 500 ppm polymer solution injection case. (*a*) Mean velocity profiles obtained at each measurement location shown along with (i) $u^+ = y^+$ line, (ii) theoretical log law for a Newtonian turbulent boundary layer velocity profile and (iii) MDR asymptote. (*b*) Reynolds stress profiles obtained at each measurement location compared to Newtonian Reynolds stress profile.

The equivalent measurements locations in the present experiment are at positions 06 and 2. The Reynolds stresses in the near-wall regions are heavily damped by the action of the polymer and this in turn affects the state of the turbulence. As the flow develops, the DRs decrease past position 2 which is reflected in the mean velocity profiles falling back into the LDR regime. The Reynolds stress profiles also start to revert back towards the Newtonian profile. The polymer loses its effectiveness as it is convected away from the wall and the DRs diminish.

Mean velocity profiles obtained for injection of 500 ppmw polymer solutions are shown in figure 10(*a*). At all measurement locations, HDRs ($> 60\,\%$) are measured with the highest being 70 % measured at position 2. At positions 06 and 1, the injected polymer stays very close to wall forming a thick layer and measurements through this layer have potentially large errors associated with them and hence the estimation of

PEO	WSR 301		
Concentration. (ppmw)	500	250	100
Q_i/Q_s	0.79	0.82	0.78
Position 06	45 %	40 %	35 %
Position 1	50 %	54 %	45 %
Position 2	69 %	38 %	34 %
Position 3	61 %	38 %	10 %
Position 4	64 %	18 %	15 %

TABLE 2. Table showing DRs measured at each measurement station for varying concentrations of injected polymer solution. All DRs are estimated to be within 10 %. Q_s is the volume flow rate in the viscous sublayer extending up to $y^+ = 11$; $Q_s = 67.3v$. Q_i is the injection rate of the polymer solution.

DRs at these locations are also more uncertain (see Hou, Somandepalli & Mungal (2006) for a detailed discussion). Further away from the wall, the log-law region changes slope, characteristic of the HDR regime, and the profiles either coincide with or lie close to the MDR asymptote. Figure 10(*b*) shows the Reynolds stress profiles that are obtained for this case. The effect of the polymer is to suppress the Reynolds stress in the near-wall region along the entire length of the flat plate. This is seen clearly at all the measurement stations as shown in the figure. As a result of the suppression of the near-wall Reynolds stresses, the locations of the peaks of the Reynolds stress profiles are also shifted away from the wall. This effect is seen in all polymer injection experiments and the magnitude of the shift increases with increasing concentration of the injected polymer solution. A compilation of the DRs obtained at each measurement location for the cases presented above is given in table 2.

Figures 11–13 show typical side view PLIF images obtained at the five measurement locations for injected polymer concentrations of 100 ppmw, 250 ppmw and 500 ppmw, respectively. The images are arranged in the order of increasing downstream distance with the first image in each set corresponding to position 06 and the last image corresponding to position 4.

Figure 11 shows the side view PLIF images obtained for the case of injection of 100 ppmw polymer solution. The PLIF images obtained at position 06 and position 1 show the presence of polymer close to the wall in the form of a thin layer. The mean concentration profiles, shown in figure 14(*a*) at these upstream profiles show a very thin layer of the polymer solution close to the wall. The magnitude of the fluctuations (figure 14*b*) in the concentration of the injected polymer is almost as high as the mean concentration profile itself. At position 2 and further downstream, the PLIF images and the mean concentration profiles show that the injected polymer is mixed into the boundary layer flow by the action of turbulence. At position 2, the measured concentration profiles show a distinct drop in the peak value close to the wall and a thickening of the concentration in the region beyond the wall. Beyond position 2, the magnitude of the fluctuations seen in the concentration also drop to almost zero giving further proof that the turbulence acts to mix the injected polymer into the flow.

Figure 12 shows the PLIF images obtained for the 250 ppmw polymer injection case. At positions 06 and 1, the injected polymer solution remains close to the wall in thin layers with very little large-scale turbulent eddies evident in the photographs.

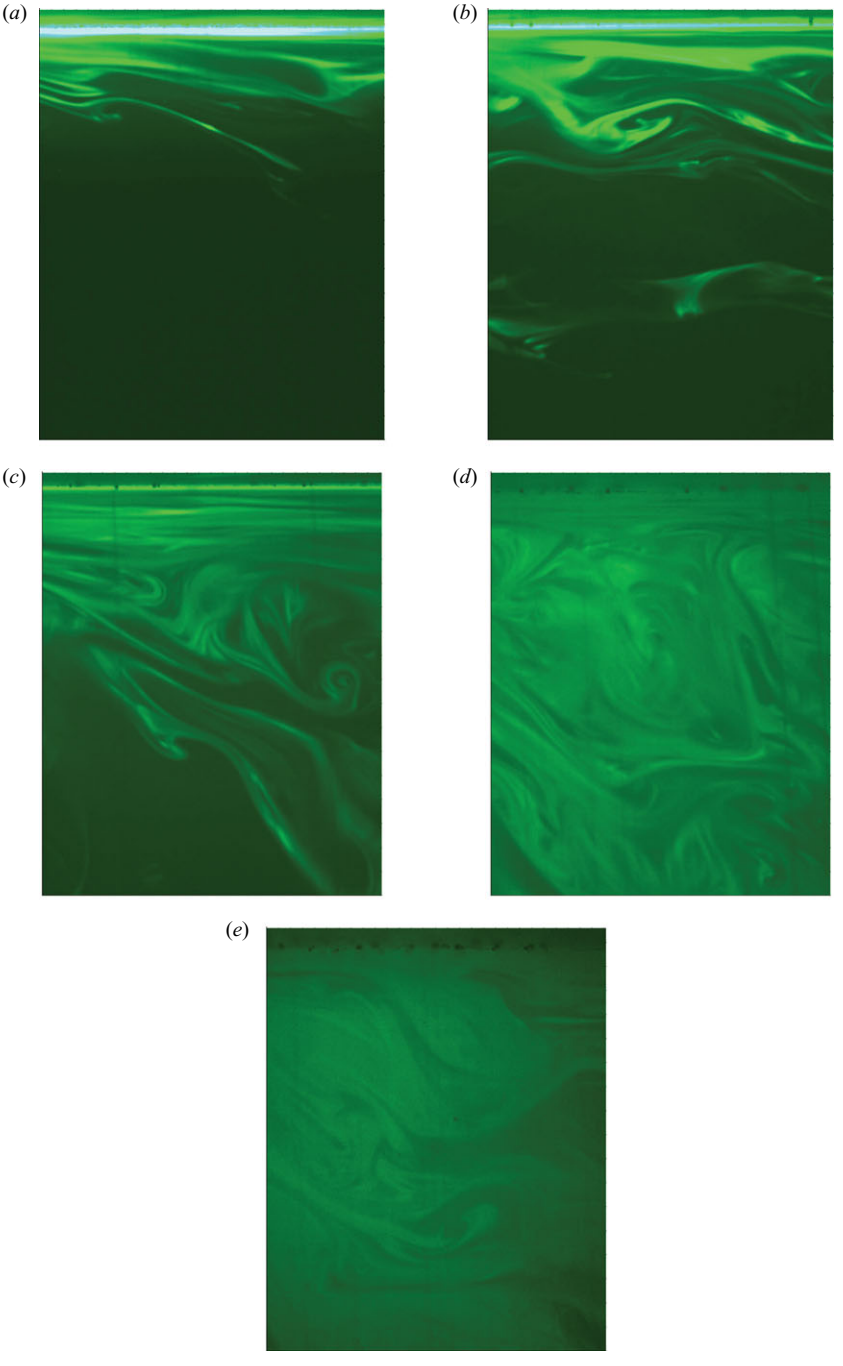

FIGURE 11. Typical PLIF images observed for the case of 100 ppm polymer solution injection. Images obtained: (*a*) at position 06, (*b*) at position 1, (*c*) at position 2, (*d*) at position 3 and (*e*) at position 4. In each case, image size is 17.5 mm $\times$ 14.3 mm (H $\times$ W).

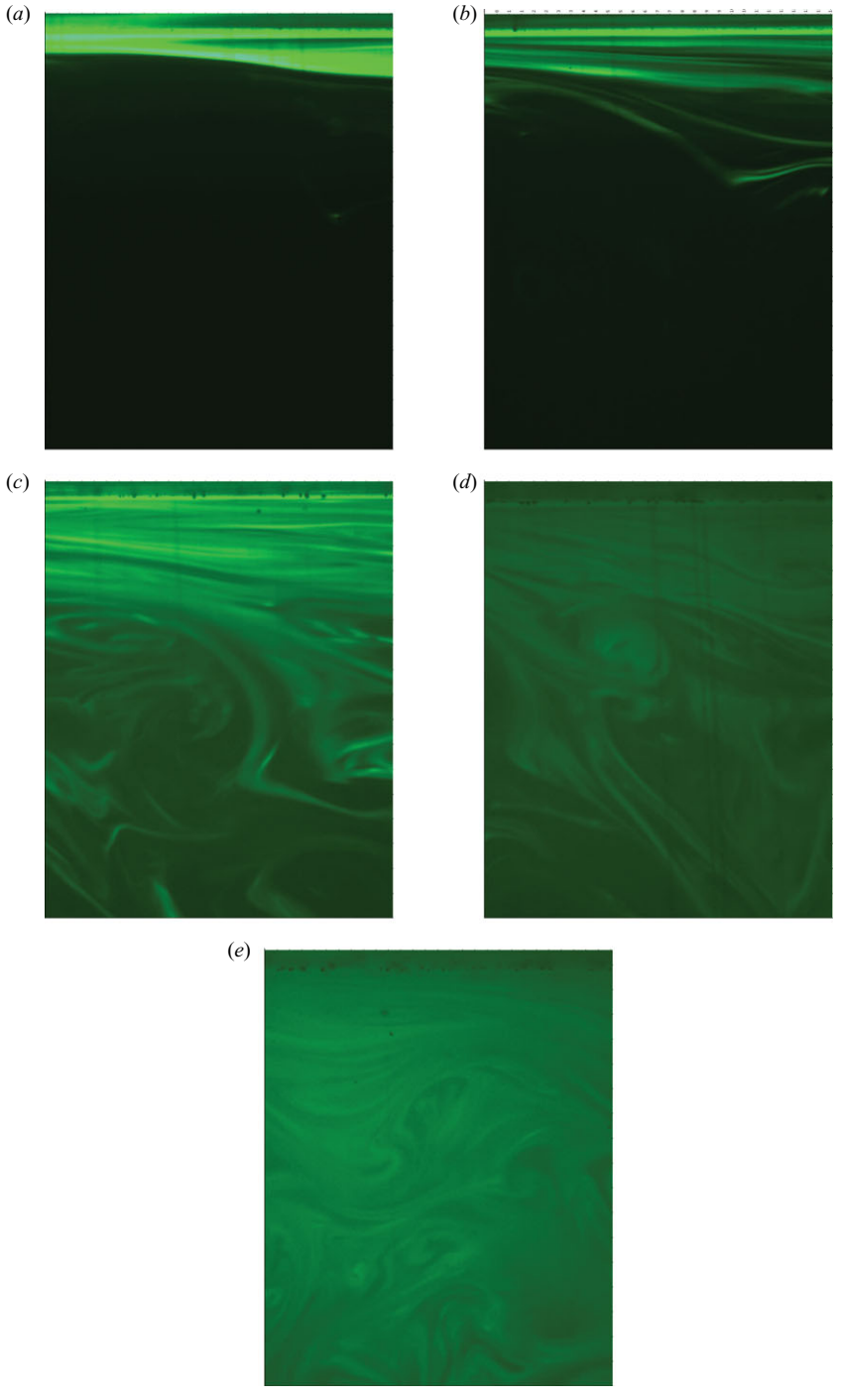

FIGURE 12. Typical PLIF images observed for the case of 250 ppm polymer solution injection. Images obtained: (*a*) at position 06, (*b*) at position 1, (*c*) at position 2, (*d*) at position 3 and (*e*) at position 4. In each case, image size is 17.5 mm $\times$ 14.3 mm (H $\times$ W)

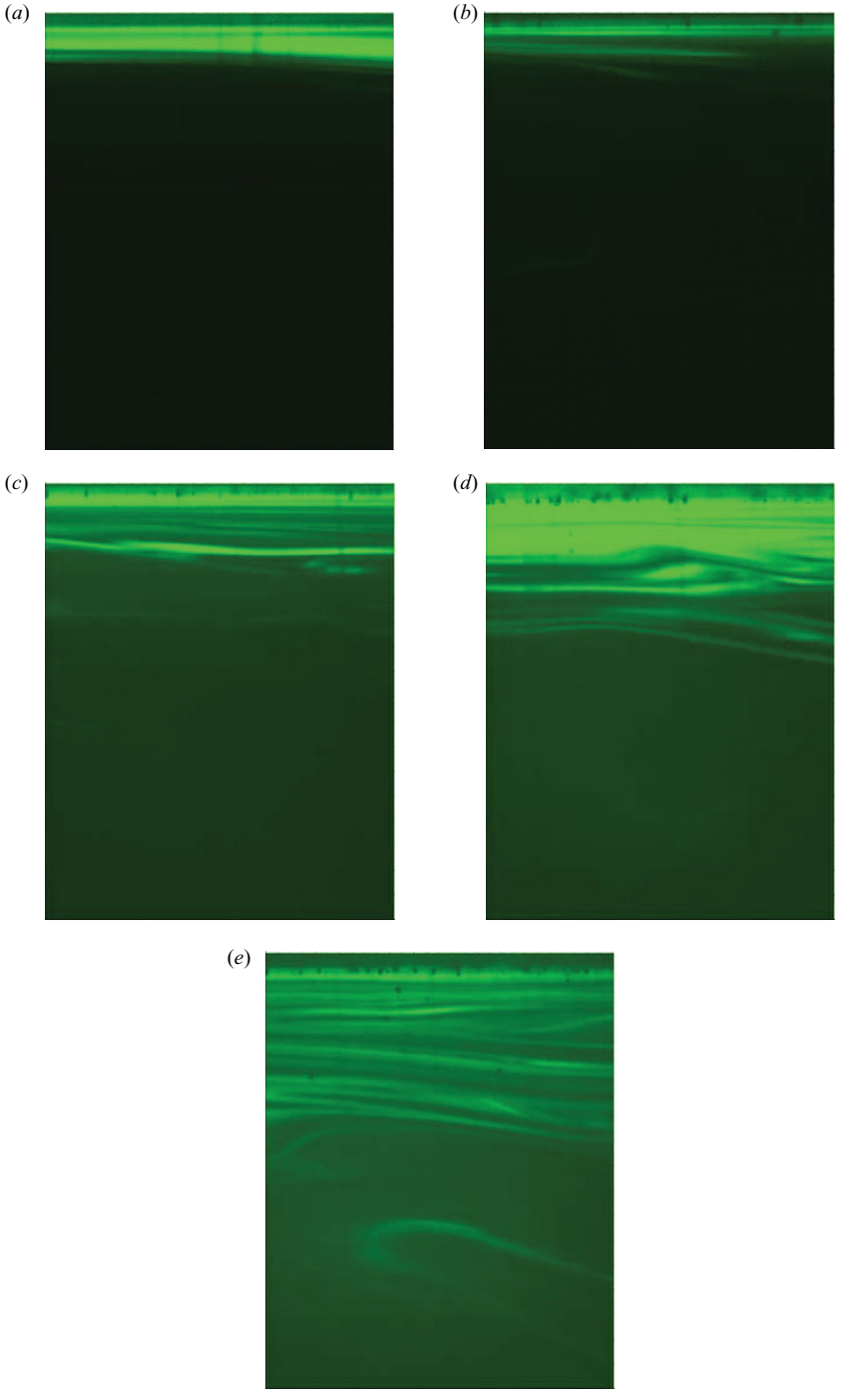

FIGURE 13. Typical PLIF images observed for the case of 500 ppm polymer solution injection. Image obtained: (*a*) at position 06, (*b*) at position 1, (*c*) at position 2, (*d*) at position 3 and (*e*) at position 4. In each case, image size is 17.5 mm × 14.3 mm (H × W)

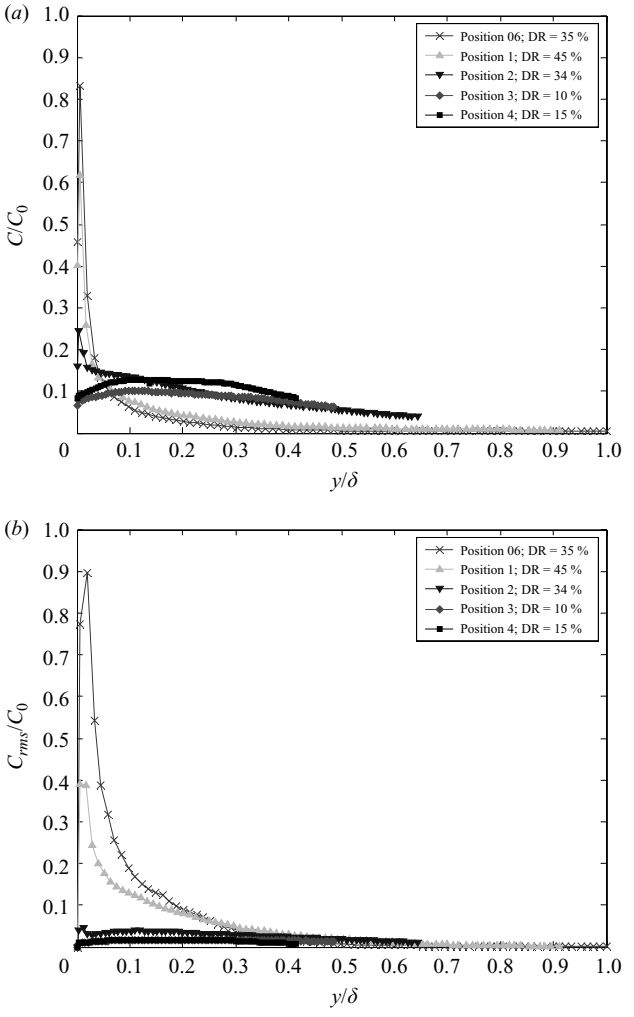

FIGURE 14. Concentration profiles obtained from PLIF measurements for the 100 ppm polymer injection case at each measurement station (as labelled in legend). (*a*) The normalized mean concentration profile; (*b*) the normalized r.m.s. concentration profile.

Further downstream, at positions 2 and beyond, the turbulence in the mean flow acts to mix the injected polymer into the mean flow as shown in the photographs in figure 12(*c–e*). Figure 15(*a*) shows the mean profile obtained in the experiment with 250 ppmw polymer solution injection. The root mean square (r.m.s.) concentration profile is shown in figure 15(*b*). As was the case with the 100 ppmw polymer solution, the mean concentration profile shows a strong peak close to the wall for positions 06 and 1. The mean concentration decays away rapidly from the peak as the distance from the wall increases with most of the polymer resident within the $y/\delta < 0.1$ region of the boundary layer. This is also clearly seen in the corresponding PLIF photographs for these locations. The concentration decays rapidly downstream of position 1 – at position 2 the relative peak measured is $C/C_0 = 0.2$ which is even smaller than the peak measured at the corresponding location for the 100 ppmw case. The r.m.s. concentration profile, at position 06, has a peak that is half as large as the

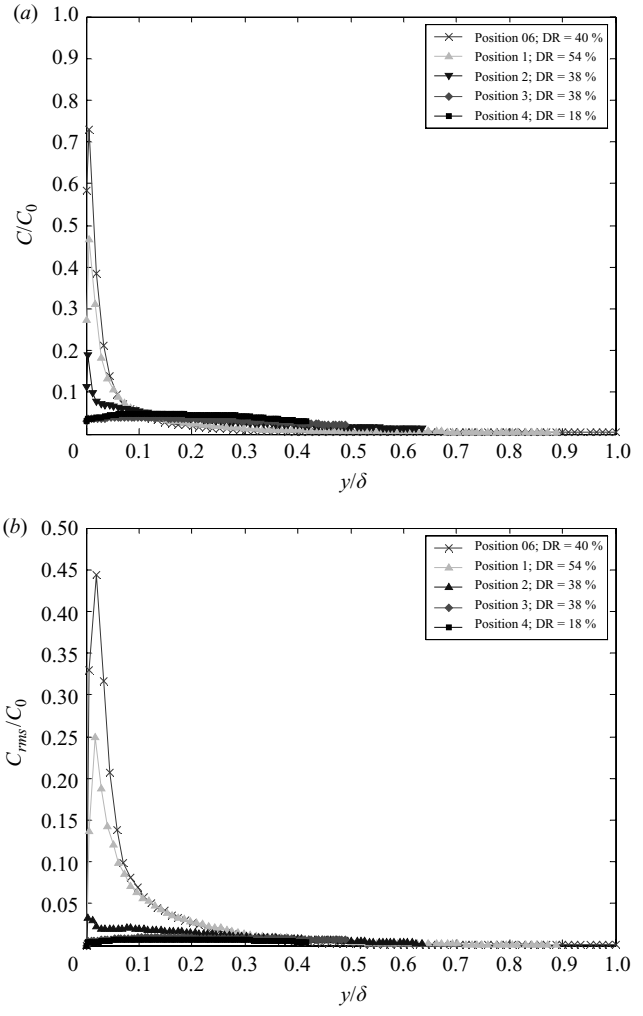

FIGURE 15. Concentration profiles obtained from PLIF measurements for the 250 ppm polymer injection case at each measurement station (as labelled in legend). (*a*) The normalized mean concentration profile; (*b*) the normalized r.m.s. concentration profile.

one seen for the 100 ppmw case indicating much less intermittency in the large-scale fluctuations of the injected polymer at this measurement station. At position 1, a similar peak is seen in the r.m.s. concentration profile with its peak magnitude being smaller than that at position 06 and also smaller than the corresponding peak for the 100 ppmw case. As the flow develops, the r.m.s. fluctuations subside, as seen in the profile obtained for position 2.

The PLIF images for the 500 ppm injection case, shown in figure 13 show that the injected polymer remains in a thin sheet close to the wall for a significant length of the test wall. There is very little large-scale turbulent dispersion seen in the images even at position 3. At position 4, some of the injected polymer solution breaks away from the wall in layers by the action of the turbulence in the mean flow. The mean concentration profile obtained in the case of 500 ppmw polymer solution injection is shown in figure 16(*a*). At position 06, the mean concentration profile shows an

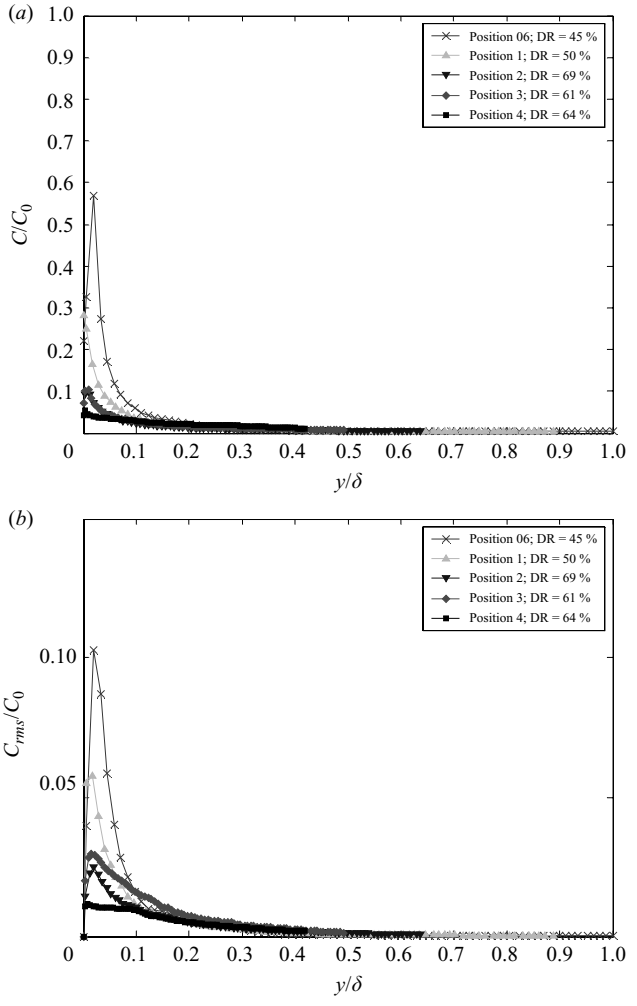

FIGURE 16. Concentration profiles obtained from PLIF measurements for the 500 ppm polymer injection case at each measurement station (as labelled in legend). (*a*) The normalized mean concentration profile; (*b*) the normalized r.m.s. concentration profile.

off-wall peak where the measured mean concentration is about 250 ppmw. This ratio of $C/C_0 = 0.5$ is lower than the mean concentration peaks seen in the lower concentration injection cases. This trend of lower peak concentration also holds at position 1 where the peak mean concentration ratio is progressively lower than those seen in the 100 ppmw case and the 250 ppmw case. The mean concentration profiles measured in the 500 ppmw case are also relatively broader than those for the lower concentration cases. The r.m.s. concentration profiles for the 500 ppmw polymer injection case are shown in figure 16(*b*). The maximum peak ratios of the r.m.s. concentrations seen in this case are small compared to the 100 ppmw and 500 ppmw case. This implies that the fluctuations in the concentration near the wall are small and less numerous. This lack of cross-stream motion of the polymer implies that most of the injected liquid flows along the wall as a layer. The PLIF images and the measured concentration profiles for the 500 ppmw injection case show that the injected polymer persists close to the wall and there is little action of turbulence to

mix it into the boundary layer. The r.m.s. concentration profiles show little fluctuation in the concentration fields that can cause the polymer to move away from the wall and mix into the outer regions of the boundary layer flow.

From the experiments and results described above, it is evident that the DRs obtained along the flat plate are dependent on the concentration of the injected polymer. The PLIF images and measurements show that the action of the injected polymer is to reduce the diffusivity of the liquid close to the wall compared to the water injection case (passive contaminant). As a result, the injected liquid remains confined to the inner near-wall region of the boundary layer and maintains a layer close to the wall. The action of the turbulence in the outer regions is to then act on this layer and mix it into the outer regions of the boundary layer. Increasing the concentration of the injected polymer solution increases this suppression of turbulent mixing and diffusion. Walker & Tiederman (1990), in their experiments in a low-speed turbulent channel flow, also showed similar results. Brungart *et al.* (1991) studied the diffusion of polymer in a flat-plate boundary layer using PLIF. Fontaine *et al.* (1992) have studied the velocity and concentration profiles obtained in a turbulent boundary layer with slot-injected polymer similar to the present set of experiments. In their experiments, they noted that the actual Reynolds stress levels for polymer injection experiments are lower than the no-injection values at all locations, as is observed here. They also observed that the suppression of the Reynolds stress extends beyond the region where the polymer is concentrated close to the wall. The PLIF measurements of the mean concentration presented here are qualitatively similar to the concentration profiles measured by Fontaine *et al.* (1992) and Brungart *et al.* (1991). Their measurements also indicate the presence of off-wall peaks in the mean concentrations measured along the flat plate. Similar off-wall peaks in mean concentration profiles were also reported by Winkel *et al.* (2009) in the PLIF measurements in their high-Reynolds-number experiments.

4. Combined PIV–PLIF measurements

The two-dimensional velocity data obtained from the PIV measurements, performed simultaneously with the PLIF, can be combined with the quantitative concentration data to calculate the streamwise and wall-normal turbulent fluxes of the concentration. These fluxes, when studied along with the concentration and velocity data separately, will enhance the mechanistic understanding of DR due to polymers. This section discusses the turbulent fluxes and derived quantities calculated by combining the PLIF and PIV measurements described in the previous sections. These turbulent fluxes and their modification as a result of the interaction of the injected polymer solution with the turbulence in the boundary layer give vital clues about the phenomenon of DR.

Concentration fluctuation fields corresponding to individual PIV vector frames are calculated by subtracting the local value of mean concentration from the concentration field frames. From these, concentration flux fields containing information about both the streamwise and wall-normal flux, at each vector location are obtained by multiplying the concentration fluctuations with the velocity fluctuations at that location:

$$cu_k(i, j) = c_k(i, j)u_k(i, j), \tag{4.1}$$

where $cu_k(i, j)$ is the concentration flux field, $c_k(i, j)$ is the concentration fluctuation field and $u_k(i, j)$ is the velocity field in the kth frame referenced. These concentration

flux fields are ensemble averaged over the 1000 frames captured to give a single frame which is then line averaged over the 64 columns to give a single concentration flux profile for both the streamwise and wall-normal flux at each measurement location:

$$< cu(i, j) >= \frac{1}{1000} \sum_{k=1}^{1000} cu_k(i, j), \tag{4.2}$$

$$< cu >= \frac{1}{64} \sum_{j=1}^{64} cu(i, j), \tag{4.3}$$

where the indices *i, j* refer to the row and column number of the quantities in each frame *k*. These concentration flux profiles are used to calculate higher order turbulence quantities such as turbulent fluxes, turbulent Schmidt numbers (Sc_T) and the total polymer flux budget in the boundary layer.

4.1. *Turbulent fluxes*

Figure 17(*a*) shows the streamwise concentration flux profile obtained for the 100 ppmw polymer solution injection. The flux has been normalized using the initial injection concentration C_0 and the local friction velocity u_τ. The graph shows the measurements obtained at the five measurements stations along the flat plate. The peak magnitude of the streamwise flux is highest at position 06 with a normalized magnitude of about 0.75. As the flow develops downstream, this peak magnitude falls to 0.35 at position 1 and to an even lower value of 0.1 at position 2. Beyond position 2, the injected polymer diffuses away from the wall and the measured streamwise flux decays to small values at position 3 and is below detectable levels at position 4. The wall-normal fluxes obtained for the same case are shown in figure 17(*b*). As in the case of the streamwise fluxes, positions 06 and 1 show a peak in the flux profile near the wall. The magnitude measured at position 06 is slightly higher than that at position 1. At position 2, the flux profile rises gradually to a peak value of 0.075 which occurs at $y/\delta = 0.35$ ($y^+ = 125$) and beyond this it decays slowly towards zero. Further downstream, the wall-normal flux diffuses into the outer regions of the boundary layer. The location of the peak in the flux profiles moves away from the wall as the downstream distance from injection increases.

The normalized streamwise flux measurements, in inner coordinates, obtained along the flat plate for an injection concentration of 250 ppmw are shown in figure 18(*a*). Similar to the 100 ppmw injection case, the peak in the profile measured at position 06 is located very close to the wall at $y/\delta < 0.05$ ($y^+ < 10$) and the profile decays rapidly at larger values of y/δ. At position 1, the peak in the measured profile moves away from the wall to $y/\delta = 0.07$ ($y^+ \sim 15$) and at position 2, the peak occurs at about $y/\delta = 0.09$ ($y^+ = 35$). The peak magnitudes measured in the 250 ppmw case are lower than those measured in the 100 ppmw case. The wall-normal fluxes measured in the 250 ppmw polymer injection case, shown in figure 18(*b*), are also about three times smaller than those measured in the 100 ppmw case.

The most striking aspect of the streamwise fluxes measured in the 500 ppmw case, shown in figure 19(*a*), is the small but non-zero magnitudes of the flux measured at all the measurement positions along the flat plate. The wall-normal fluxes measured in the case of 500 ppmw injection experiment, shown in figure 19(*b*), are noisier in the near-wall region compared to the 100 ppmw and the 250 ppmw case. The peak magnitudes of the fluxes measured in this experiment, along the flat plate are

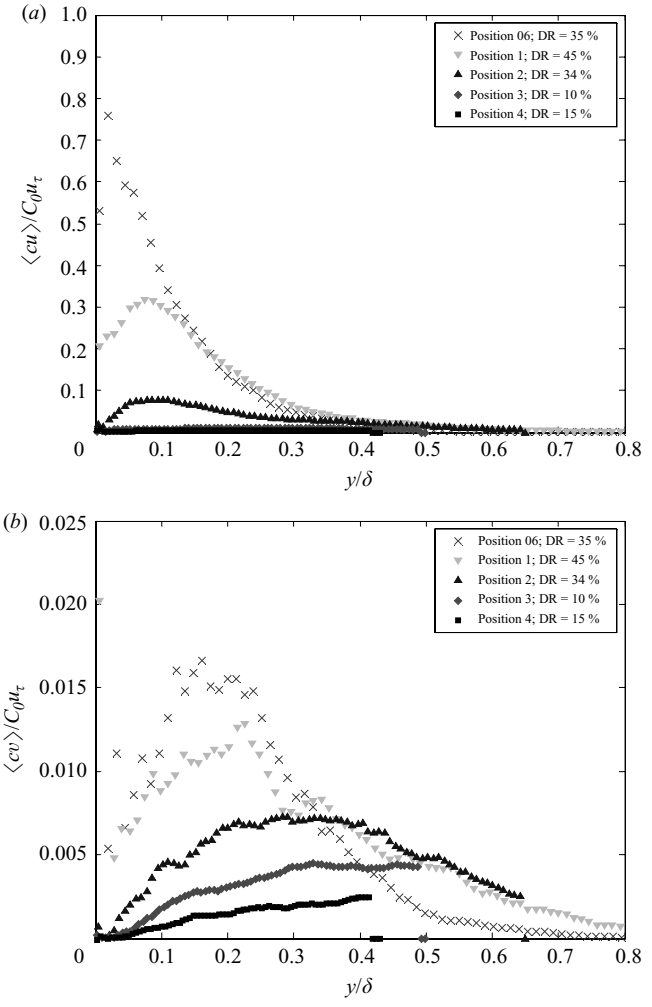

FIGURE 17. Turbulent Fluxes measured at different measurement stations in the 100 ppm polymer injection case. (*a*) The streamwise turbulent flux; (*b*) the wall-normal turbulent flux. Both quantities normalized by the initial injection concentration and friction velocity.

an order of magnitude lower than those measured in the experiments with lower polymer concentration injections.

It is instructive to study how the streamwise fluxes, in the different concentrations tested, evolve across several measurement stations relative to each other (figure 20*a*). The profiles show clearly how the concentration of the injected solution influences the decay rates of the streamwise fluxes. The 100 ppmw case, identified by the square symbols, decays rapidly from position 06 to position 2, whereas the 500 ppmw case, does not show any significant decay of the streamwise flux between the same two positions. The 250 ppmw case, as expected, falls between the two extremes comparatively. The location of the peaks of the profiles also can be compared in the same graph. As the concentration of the injected solution increases, the peaks in the flux profiles remain closer to the wall as the distance from injection increases. The evolution of the wall-normal fluxes along the flat plate, for the different concentrations tested, relative to each other is shown in figure 20(*b*). As can be seen from the graph,

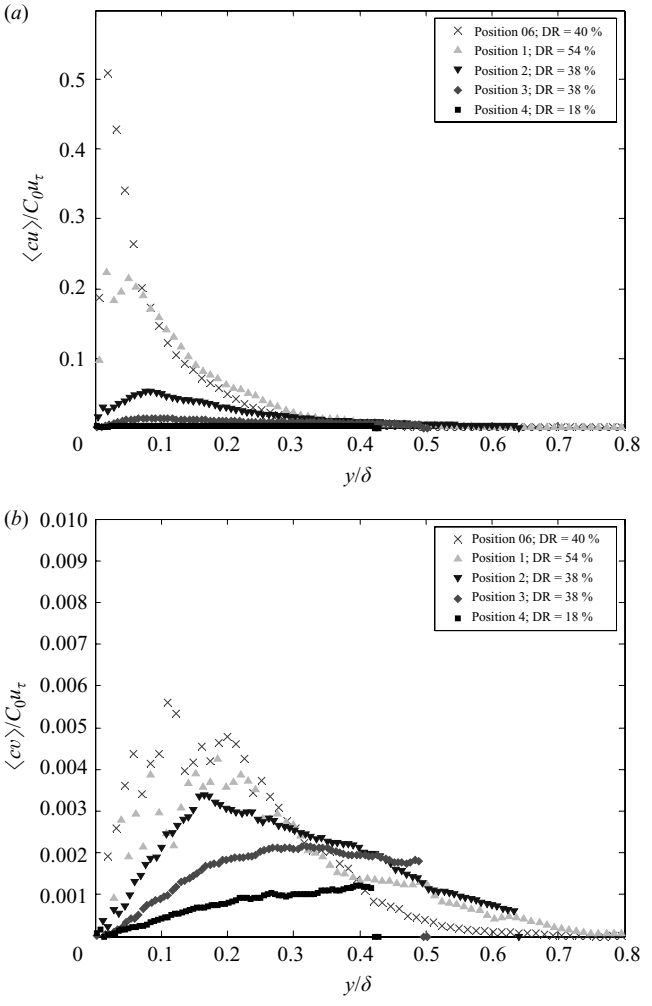

FIGURE 18. Turbulent fluxes measured at different measurement stations in the 250 ppm polymer injection case. (*a*) The streamwise turbulent flux; (*b*) the wall-normal turbulent flux. Both quantities normalized by the initial injection concentration and friction velocity.

the 100 ppmw case, decays the fastest among the three cases, with the peak magnitude dropping significantly compared to the other cases. The movement away from the wall, of the peak in the wall-normal flux profile, is also very clearly evident in this case. The 250 ppmw case shows a smaller decay rate along the flat plate. The 500 ppmw case, with its very low flux magnitudes, shows the least movement, both in terms of change in magnitude and also the location of the peak of the profile.

The local maximum concentration of the injected solution can also be used as a normalization factor for the streamwise fluxes and this provides a clearer picture of the flux as the measurement is not artificially reduced in magnitude by the initial injection concentration. The evolution of the fluxes along the flat-plate measurement location, normalized with their respective local maximum concentrations, is shown in figure 21. The graphs also include the measurements made for the case of water injection so that the polymer injection cases can be compared against it. The streamwise fluxes measured in water (figure 21*a*) decay the fastest, with no measurable flux seen beyond

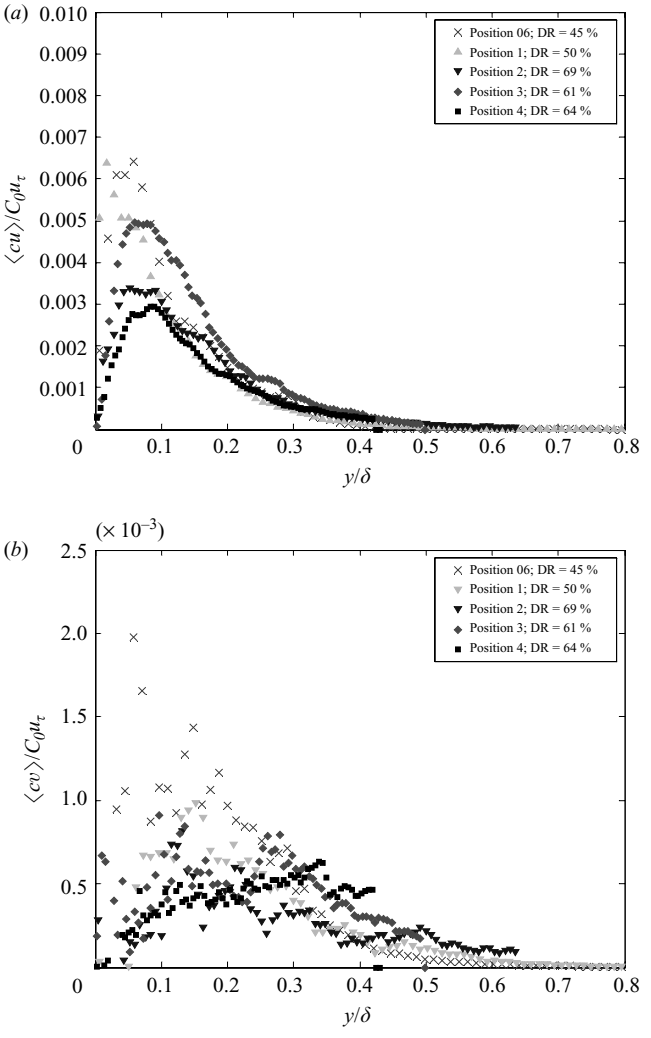

FIGURE 19. Turbulent Fluxes measured at different measurement stations in the 500 ppm polymer injection case. (*a*) The streamwise turbulent flux; (*b*) the wall-normal turbulent flux. Both quantities normalized by the initial injection concentration and friction velocity.

position 1. In the polymer injection cases, specifically the 100 ppmw and the 250 ppmw cases, the decay is much slower with the 100 ppmw case showing significant flux at position 2 and the 250 ppmw case at position 3. In the case of the 500 ppmw injection, the fluxes increase in magnitude along the length of the plate. The fluxes measured at the downstream locations labelled 3 and 4 are greater than those measured for the 100 ppmw and the 250 ppmw case at the first measurement location. In the graph (figure 21*b*) comparing the wall-normal fluxes, the cases with polymer injection show much lower wall-normal fluxes compared to the case with water injection. The water injection case also shows a decay of the flux with increasing downstream distance whereas the polymer injection cases show an increase in the flux with increasing downstream distance. This growth is most noticeable in the 250 ppmw case. The 500 ppmw case fluxes are much smaller in magnitude and hence the growth is not

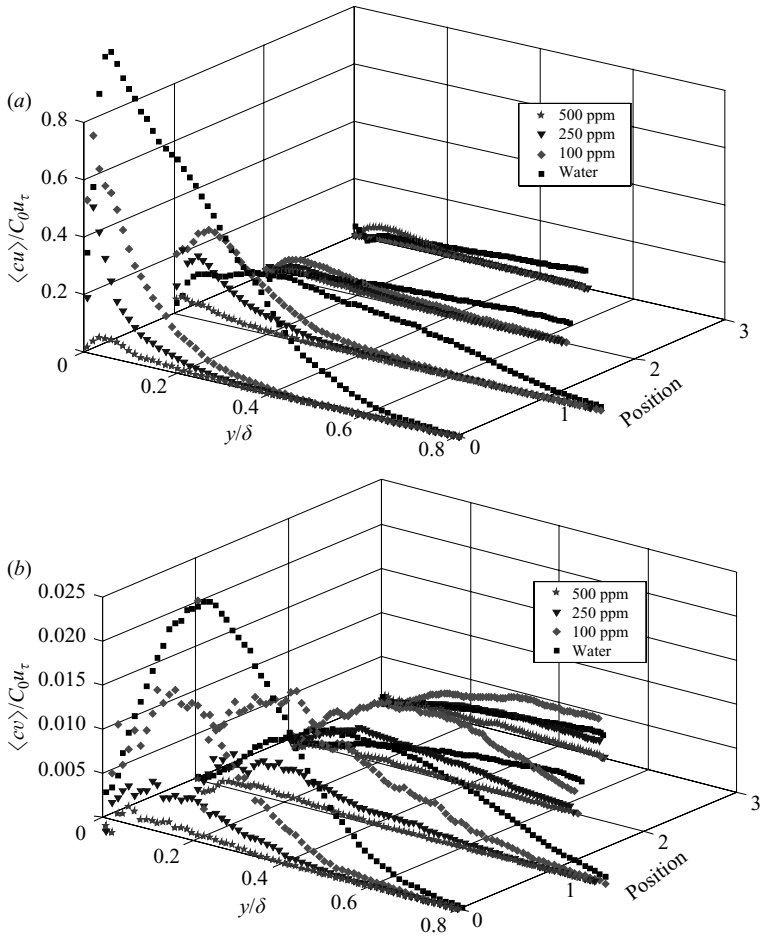

FIGURE 20. Evolution of turbulent fluxes along the flat plate for the water injection and polymer injection cases. (*a*) The streamwise fluxes; (*b*) the wall-normal fluxes. Both quantities normalized by the initial injection concentration and friction velocity.

very apparent. The wall-normal shift of the location of the peaks in the profiles also is retarded with increasing concentration.

The injection of polymer causes the turbulence fluxes – both streamwise and wall normal – to be reduced greatly. This drastic reduction in the turbulence fluxes is also accompanied by a large reduction of Reynolds stress (Hou *et al.* 2008). The wall-normal fluxes control the processes by which mass and momentum is transferred away from the near-wall region and into the mean flow. The measurements show that this wall-normal flux is greatly reduced due to the action of polymer. This suppression of the wall-normal flux is greatest at the highest concentration of polymer injection and decreases with decreasing DR. Similar behaviour of the wall-normal flux was also noticed by Kawaguchi *et al.* (2002) who studied the DR and heat transfer effects of injected surfactant additives in channels and pipes. Li *et al.* (2001) and Li, Kawaguchi & Hishida (2003) also showed a similar reduction in the wall-normal flux in their experimental study on heat transfer effects of drag-reducing additives in channels. This suppression of the wall-normal flux directly leads to the suppression of turbulent mixing of the injected polymer. As a result, more of the injected polymer

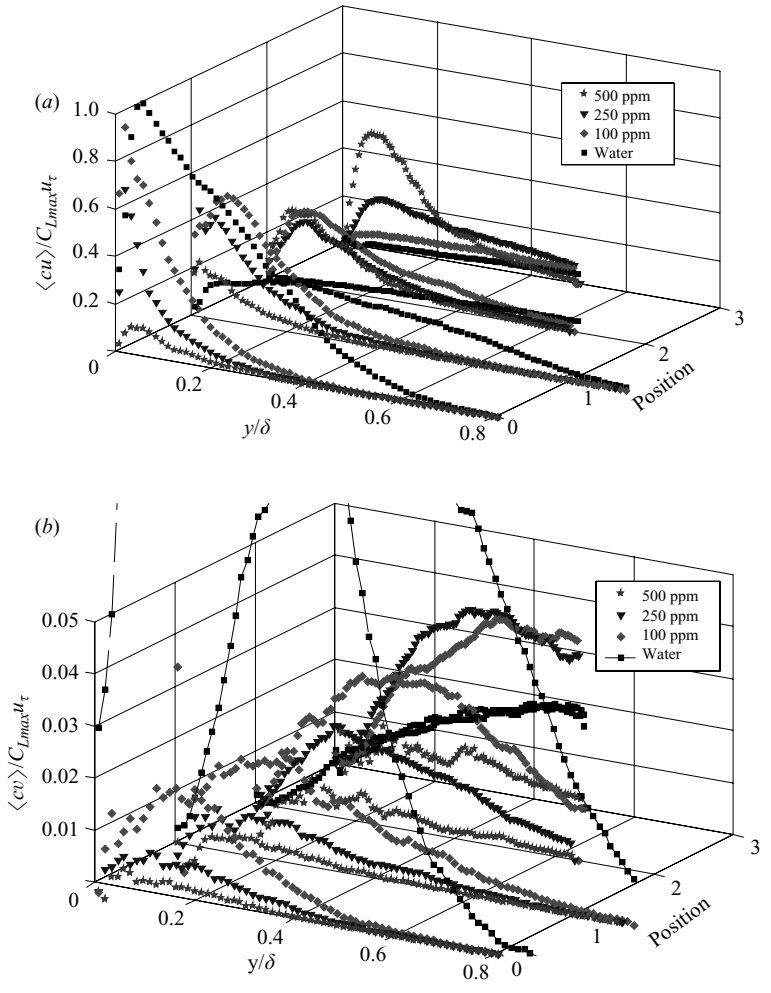

FIGURE 21. Evolution of turbulent fluxes along the flat plate for the water injection and polymer injection cases. (*a*) The streamwise fluxes; (*b*) the wall-normal fluxes. Both quantities normalized by the measured local maximum concentration and friction velocity.

solution is retained close to the wall and flow next to it as a layer as was seen in the mean and r.m.s. concentration profiles seen in the earlier sections. Gupta, Sureshkumar & Khomami (2005) have studied passive scalar transport in a polymer drag-reduced turbulent channel flow computationally. They showed that the wall-normal fluxes decreased with increasing DR. They also noted that the peak in the wall-normal flux profiles move away from the wall with increasing DR. The trends they observed are very similar to those measured in the present set of experiments.

4.2. *Polymer flux budget*

An estimate of the amount of the polymer solution present in the boundary layer in the tunnel can be made by summing the total streamwise polymer flux. This flux can then be compared with the amount of polymer injected into the boundary layer to ensure that the injected polymer is accounted for in the polymer concentration

Q	Water	100 ppm	250 ppm	500 ppm
Based on injection rate	74.9	82.4	74.9	77.7
Measured at position 06	79.4	80.9	72.0	66.9
Measured at position 1	73.0	82.6	69.9	73.3

TABLE 3. Estimated polymer flux at positions 06 and 1 for the different cases tested. Polymer flux estimated from the injection rate is shown in the first row for each case.

measurements. The polymer flux Q in the boundary layer is given by

$$Q = \int_o^\delta [C(y)U(y) + c(y)u(y)]\,\mathrm{d}y, \tag{4.4}$$

where $C(y)$ is the mean concentration, $U(y)$ is the mean velocity, $c(y)$ is the concentration fluctuation and $u(y)$ is the streamwise velocity fluctuation, all measured at a distance y from the wall. This quantity is calculated at positions 06 and 1 for all the cases tested – water injection, 100 ppm, 250 ppm and 500 ppm polymer injection experiments. Table 3 shows a comparison of volume flux of the injected solution based on the injection rates and the polymer flux as calculated from (4.4). As can be seen from the table, the volume of liquid injected is recovered fairly accurately in the boundary layer for the water injection, 100 ppm and 250 ppm polymer injection cases. The 500 ppm case shows the highest discrepancy at position 06 with a deficit of about 15 % in the measured polymer flux. This is possibly due to the velocity mismatch in the region very close to the wall where the injected solution forms a layer and does not mix well into the outer flow. The high concentration of the fluorescent dye in that region and, as a result, the incorrect estimation of the polymer concentration could also be a factor in this deficit of polymer measured. This test also gives indirect confirmation that the technique and analysis used to measure the polymer concentration using PLIF are sound and accurate.

4.3. *Turbulent Schmidt number*

The Sc_T, which is a ratio of the momentum eddy diffusivity to the concentration eddy diffusivity, can be defined as

$$Sc_T = \frac{\overline{uv}(\mathrm{d}C/\mathrm{d}y)}{\overline{cv}(\mathrm{d}U/\mathrm{d}y)}, \tag{4.5}$$

where $\overline{uv}$ is the Reynolds shear stress, $\overline{cv}$ the turbulent wall-normal flux, $\mathrm{d}C/\mathrm{d}y$ the gradient of the mean concentration and $\mathrm{d}U/\mathrm{d}y$ the gradient of the mean velocity in the flow. The Sc_T is a measure of the relative intensities of the turbulent diffusivities of momentum and concentration (mass) in a flow. The gradients of the mean velocity and the mean concentration are obtained by differentiating the mean velocity and concentration profiles, respectively, using a second-order central difference formula,

$$\frac{\mathrm{d}f_i}{\mathrm{d}y} = \frac{(y_{i-1} - y_i)^2(f_{i+1} - f_i) - (y_{i+1} - y_i)^2(f_{i-1} - f_i)}{(y_{i-1} - y_i)^2(y_{i+1} - y_i) - (y_{i+1} - y_i)^2(y_{i-1} - y_i)}. \tag{4.6}$$

The differentiation is an inherently noisy process because the derivatives accentuate the noise in the signal. To eliminate most of the noise, the data was smoothed by averaging each point with its two nearest neighbours (Elkins 1997).

As explained earlier, the $\overline{cv}$ (wall-normal flux) profiles are also noisy and to reduce the uncertainty in the calculations for the Sc_T, the normalized wall-normal flux profiles

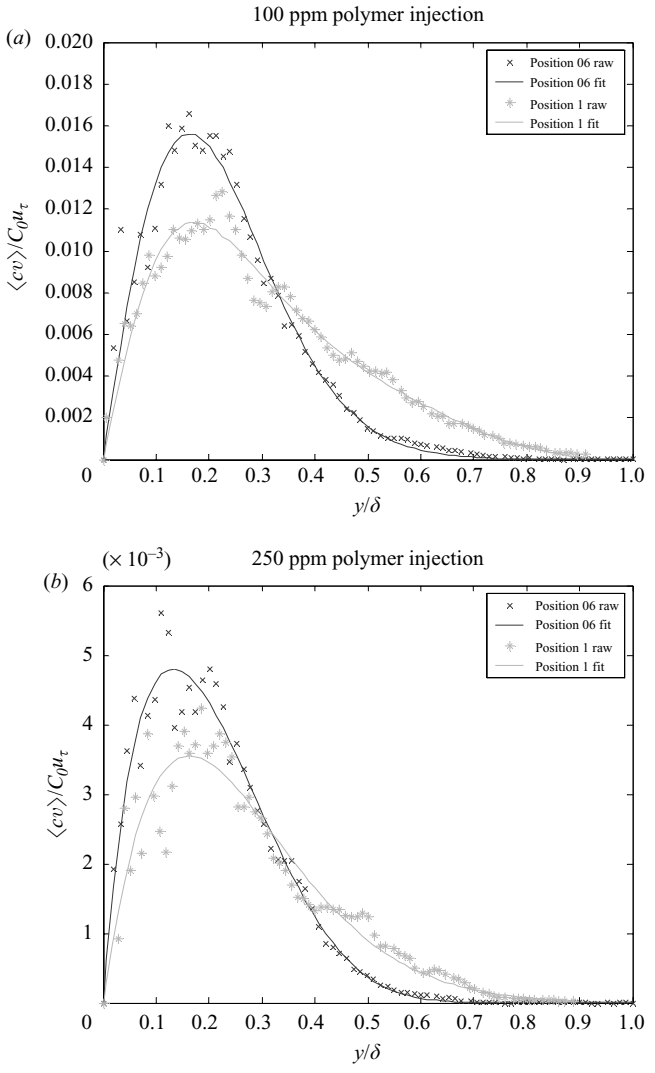

FIGURE 22. Curve fits to the measured wall-normal flux at positions 06 and 1 for (*a*) 100 ppm polymer injection case and (*b*) 250 ppm polymer injection case.

were curve-fitted. A curve fit of the form

$$y = x * \exp(a + bx + cx^2) \tag{4.7}$$

was found to universally fit the wall-normal flux profiles obtained with the correct trends near the wall and at the edge of the boundary layer. Figure 22 shows a comparison of the raw wall-normal flux data and the fitted curves for the cases of 100 ppmw (figure 22*a*) and 250 ppmw (figure 22*b*) at positions 06 and 1.

Figure 23 shows the Sc_T profiles obtained for the water injection case. The turbulent Schmidt number profiles at all locations are relatively flat with a magnitude of unity over a large portion of the boundary layer. The measurements at positions 06 and 1 very clearly show this expected magnitude. Positions 2 and 3 profiles are a little noisier, especially close to the wall and in the free stream. These profiles also show a peak in the Sc_T close to the wall. This peak and the increasing noise are a numerical

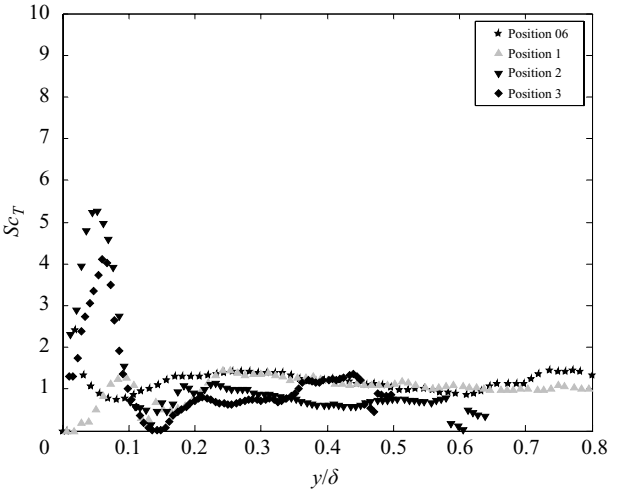

FIGURE 23. The Sc_T profiles calculated at each measurement location along the flat plate for the water injection case.

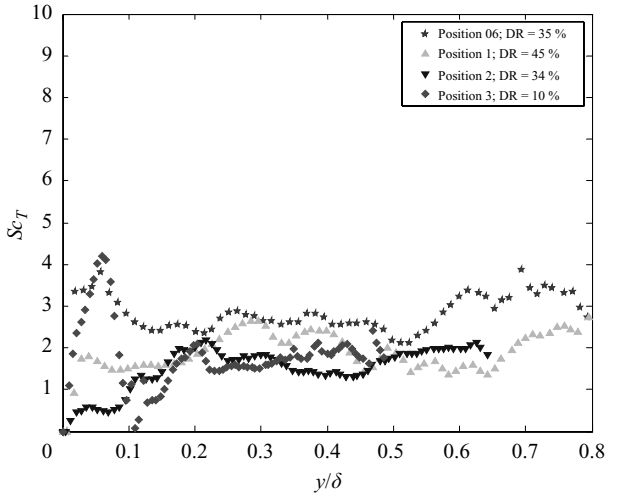

FIGURE 24. The Sc_T profiles calculated at each measurement location along the flat plate for the 100 ppm polymer injection case.

artifact of the errors associated with the numerical differentiation used to calculate the gradient of the mean concentration – a quantity that has low signal to noise at these downstream locations due to turbulent dispersion and mixing away of the injected dye.

Figure 24 shows the Sc_T profiles obtained for the 100 ppmw polymer injection case. At position 06, the average value of Sc_T is 2.7 which reduces to 2 at position 1. As the flow develops, further downstream, at position 2, the average Sc_T value decreases to 1.5 indicating that the flow tends to become more 'water-like' as the polymer is mixed by the turbulence and loses its effectiveness at DR. At position 3, the Sc_T profile shows a near-wall peak, similar to that observed in the case for water injection.

The Sc_T profiles obtained in the 250 ppmw polymer solution injection case are shown in figure 25. At position 06, the average Sc_T estimated is 3.1 and is higher

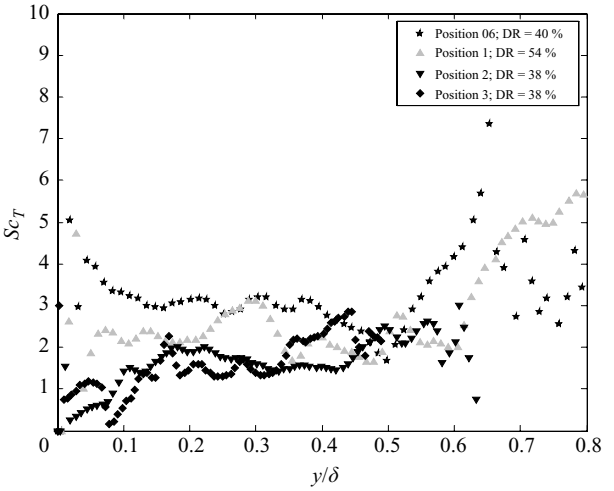

FIGURE 25. The Sc_T profiles calculated at each measurement location along the flat plate for the 250 ppm polymer injection case.

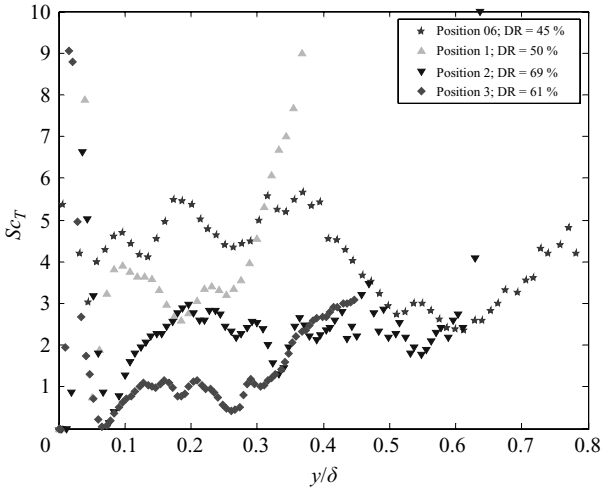

FIGURE 26. The Sc_T profiles calculated at each measurement location along the flat plate for the 500 ppm polymer injection case.

than the Sc_T obtained at the same position for the 100 ppmw case. At position 1, this value decreases to 2.4 and at position 2, it is estimated to be about 1.8. The Sc_T values estimated at position 3 are similar to those obtained at position 2. The Sc_T values estimated in the 250 ppmw case are higher than the values estimated for the 100 ppmw case at the corresponding locations. This is indicative of the polymer action being more effective in the 250 ppmw case compared to the 100 ppmw – a fact that is also borne out by the higher DRs observed in the 250 ppmw case.

The 500 ppmw case Sc_T estimates show the largest variation in the range of Sc_T seen in an experiment (figure 26). At position 06, the average Sc_T estimated is about 5 in the inner regions of the boundary layer with the value dropping to 3.5 at position 1. At position 2, the Sc_T estimated drops to about 2.5. The Sc_T measured in this experiment are also the highest measured in all the experiments at each position.

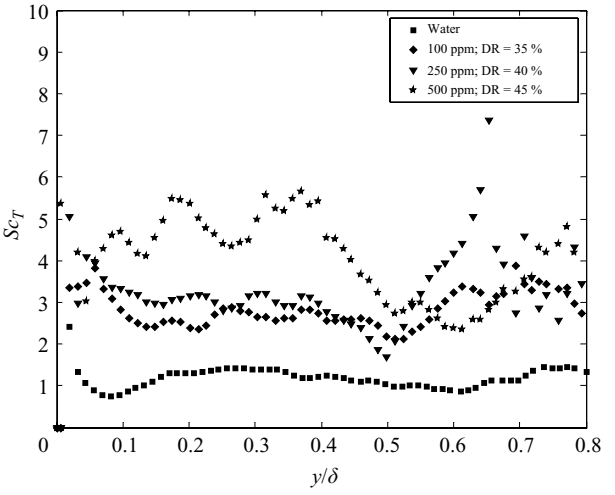

FIGURE 27. Comparison of Sc_T profiles at position 06 for the different water injection and polymer injection cases tested.

Due to the relatively low mixing rates of the injected polymer seen in the near-wall regions, the fluctuations of concentration and concentration based quantities are less converged and this is reflected in the high variations seen in the estimated Sc_T at each location.

4.4. *Effect of concentration on turbulent Schmidt number*

A comparison of the Sc_T, at each measurement location, across the various experiments performed gives an idea of the effect of polymer concentration on the turbulent fluxes at similar flow conditions. Each experiment can also be compared and contrasted with the others to bring out the similarities and differences in them.

The Sc_T profiles measured, at position 06, for water injection and the polymer injection cases are shown in figure 27. The profile for water is flat and has an average magnitude of 1, as is expected for a Newtonian flow. The profile for the 100 ppmw case shows an average value of 2.7 while, for 250 ppmw, it is 3.1. The profile for the 500 ppmw case, with an average value of 5, shows the largest amount of fluctuation compared to the other cases. The increasing value of the Sc_T, with increasing polymer concentration, is a direct result of the increased effect of the polymer on the turbulence in the flow. At position 1, as shown in figure 28, the water injection case shows the expected average value of 1 for the Sc_T. The Sc_T increases progressively with increasing concentration of the injected solution with average values of 2, 2.4 and 3.5 measured for the 100 ppmw, 250 ppmw and 500 ppmw cases, respectively.

Figure 29 shows the Sc_T profiles obtained at position 2 for the different experiments conducted. The water injection case shows an average value of 1, as expected, which increases to 1.5 in the 100 ppmw and 1.8 in the 250 ppmw polymer injection cases. The average Sc_T value measured for the 500 ppmw case at this location is 2.5 with the measurement being noisier than that in the cases with lower polymer concentrations tested. The Sc_T profiles estimates at position 3 are shown in figure 30. All the profiles, including the water injection case, are noisier than their corresponding profiles at the upstream measurement locations. This is due to the lower signal to noise ratios measured as a result of the mixing of the injected dye into the flow by the turbulence.

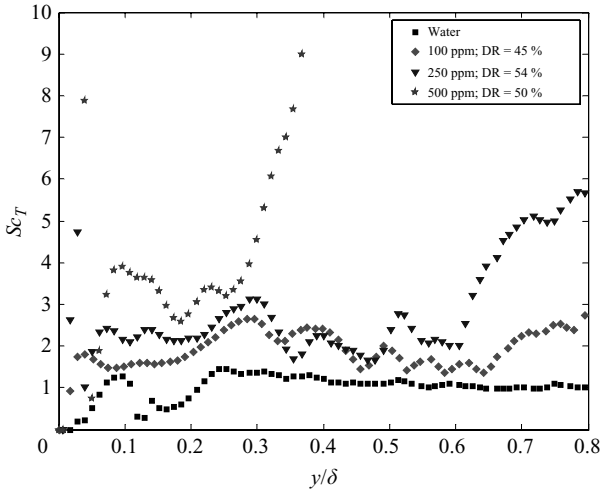

FIGURE 28. Comparison of Sc_T profiles at position 1 for the different water injection and polymer injection cases tested.

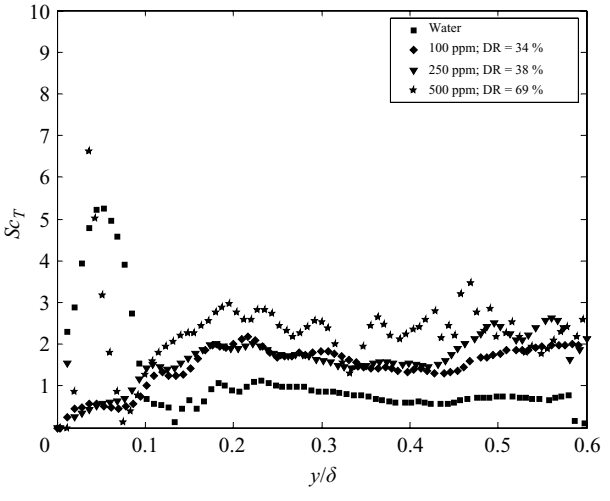

FIGURE 29. Comparison of Sc_T profiles at position 2 for the different water injection and polymer injection cases tested.

Across the cases tested, the Sc_T values at this location show much less variation in their magnitude. The average Sc_T value measured lie between 1 and 2 for all the cases tested. Due to the low signal to noise ratio, which is amplified by the lack of mixing of the injected solution into the outer regions of the boundary layer in the high polymer concentration cases, the Sc_T values may be underestimated.

The Sc_T estimated from the turbulent fluxes show quantitatively the suppression of the mass flux from the near-wall regions in the boundary layer. For the polymer injection experiments, the Sc_T increase with increasing concentration of the injected solution. The additional polymer solution interacts with the turbulence and suppresses it such that the wall-normal fluxes are inhibited severely and, as a result, the effective Sc_T is increased. The computational results obtained by Gupta *et al.* (2005) who calculated turbulent Prandtl numbers for their flow show similar results. The Sc_T

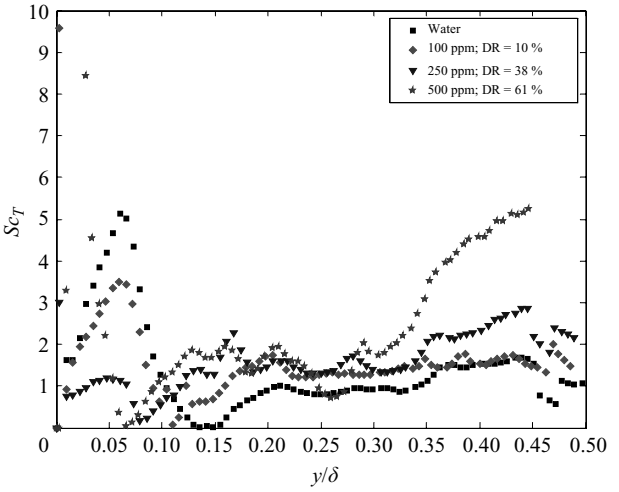

FIGURE 30. Comparison of Sc_T profiles at position 3 for the different water injection and polymer injection cases tested.

reported here which is analogous to the turbulent Prandtl number have the same magnitude and the trends observed with increasing DR and concentrations are also similar.

The large magnitude of Sc_T in the polymer drag-reduced flow implies that the momentum eddy diffusivity is large compared to the concentration (mass) eddy diffusivity. Due to this, the injected polymer solution experiences less action of the turbulence that mixes it into the outer regions of the boundary layer. However, the effect of the polymer is felt far beyond the wall, transmitted by the change in momentum. This is also seen in the modification of the turbulence fluxes. The wall-normal flux, which is responsible for mixing of fluid away from the wall, is greatly reduced by the action of the polymer. As a result, the injected polymer tends to remain where it was injected, close to the wall, along the flat plate for much longer downstream distances. This also helps the DR as this layer of injected polymer tends to act like a reservoir for drag-reducing polymer in the downstream regions of the flow where the polymer depletes by the action of the modified turbulence.

Combining the results from all the experiments presented here gives an overall idea of the DR due to the injection of dilute polymer solutions. The Sc_T combines both the velocity statistics and the concentration statistics into a single quantity. The variation of Sc_T with DR, as seen from the various experiments presented here, is shown in figure 31. In this figure, the Sc_T estimated at a location on the flat plate is plotted against the DR observed at that location, for all measurement locations and experiments performed. Also shown in the plot is a line that approximates the trend obtained from the data plotted. On the lower end of the DR scale, the Sc_T values asymptote to a value close to 1, as is expected for a purely Newtonian flow. In a flow with little or no DR, the Sc_T needs to change only a little to see a noticeable increase in the DR. As DR increases, the Sc_T also increases with a DR of 70 % corresponding to a Sc_T of approximately 4.5. At higher DRs, based on the increased slope of the trend line, the rate of change of DR is lower for a given change in the Sc_T compared to that at LDRs.

Finally, figure 32 is provided as a means to consolidate the present findings along with those of Hou *et al.* (2008), where the figure is intended to help in summarizing

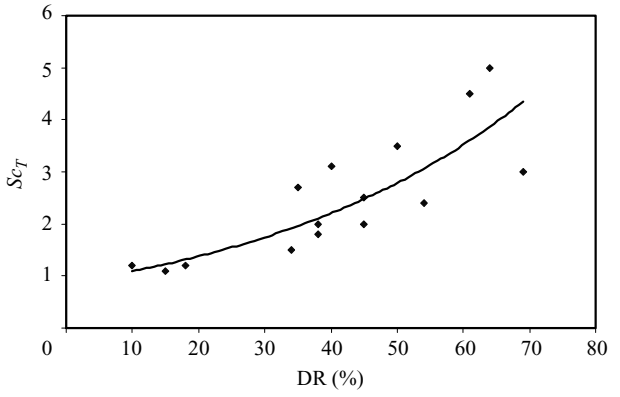

FIGURE 31. Variation of Sc_T with DR observed. Data points from all the experiments presented are plotted together. Also shown is a line approximating the observed trend in the Schmidt number increase with DR.

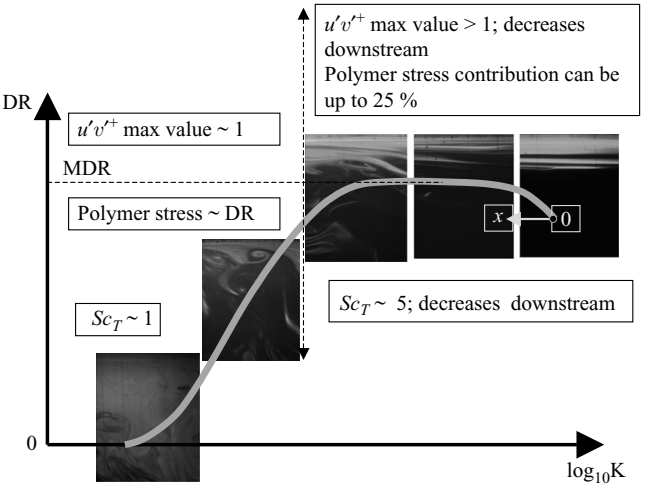

FIGURE 32. Summary of findings from Hou *et al.* (2008) and present results in DR versus $\log_{10}K$ plot.

various observation of the flow at different conditions. A general collapse of DR data is given in a plot of DR versus $\log_{10}(K)$ (Vdovin & Smol'yakov 1981; Petrie & Fontaine 1996; Petrie *et al.* 2003) where DR is the drag reduction; $K = (QC_m)/(\rho U X_S)$, where Q is the volume flux of injected polymer solution per unit span, C_m is the mass concentration of polymer solution (i.e. kg m^{-3}), ρ is the water density, U is the free-stream velocity and X_S is the downstream measurement location. Winkel *et al.* (2009) present a similar plot summarizing the data from their experiments. Their data is also presented as a graph of C_M versus K where C_M is the maximum concentration measured in the near-wall region in their experiments.

Following Hou *et al.* (2008), figure 32 is idealized in that it assumes there exists a 'universal curve' in DR versus $\log_{10}(K)$ space for a given type of polymer and injector arrangement. The line shows an example of the DR development following high polymer concentration injection. Beginning at the right, we see the development, steady-state and depletion regions depicted. In the first two regions the normalized

Reynolds shear stress exceeds unity, an indication of non-equilibrium flow in the boundary layer, while in the depletion region the polymer stress becomes proportional to the DR. To these earlier observations we have added typical flow visualization images which capture the character of the flow in these three regions. In addition, we indicate the change in the Sc_T, consistent with the suppressed turbulent fluxes, from the injection location to far downstream where the flow reverts to water-like behaviour.

5. Conclusions

PLIF measurements of the injected solutions in the turbulent boundary layer were performed to study the spread and distribution of the injected polymer in the boundary layer along a flat plate. Qualitative imaging showed that in the case of water injection, the dye, and hence the injected solution is rapidly mixed into the outer regions of the boundary layer by the action of turbulence. In the case of polymer injection, the turbulence in the near-wall region is suppressed and most of the polymer tends to remain close to the wall along the length of the plate. The liquid at the outer edges of this polymer layer is mixed into the outer regions by the action of the reduced turbulence in the flow and this leads to a gradual reduction in the amount of polymer in the near-wall region. As the concentration of the injected polymer solution increases, the dispersion of the injected polymer due to turbulence is reduced.

Quantitative measurements of the mean and r.m.s. concentration profiles showed that the polymer greatly suppressed the turbulent dispersion in the near-wall region. The mean concentration profiles, in all the polymer injection cases, showed that the injected solutions, though diffusing slowly, tend to remain close to the wall – within about 30 % of the local boundary layer thickness. Increase in concentration of the injected polymer causes the r.m.s. fluctuations to decrease in magnitude and the profiles show an off-wall peak that forms downstream of injection and is carried along the length of the plate.

Velocity data obtained from PIV and the simultaneously obtained concentration data from PLIF was combined to calculate the streamwise and wall-normal fluxes. The action of the polymer is to reduce the streamwise fluxes in the boundary layer with the magnitude of the suppression increasing with concentration. The decay rate of the fluxes is also modified by the presence of the polymer. For lower concentrations of the injected polymer solution, the streamwise flux rapidly decays along the length of the plate whereas for higher concentrations, such as the 500 ppmw case, though the flux magnitude is very low, the flow maintains this flux magnitude over long downstream distances in the boundary layer. The wall-normal flux controls the dispersion of the injected solution and it is seen that the polymer very effectively reduces this wall-normal flux. This reduction in the wall-normal flux causes the injected liquid to be mixed less effectively in the flow. As a result, the injected liquid continues to reside in the near-wall regions of the flow as was measured in the mean concentration profiles. The wall-normal flux profiles measured are low, close to injection. Further downstream, as the polymer begins to mix and lose its effectiveness, the magnitude of the fluxes measured increase and the location of the peak in the profile also moves away from the wall showing an increase in the wall normal flux and mixing in the boundary layer.

For the case of water injection, the computed Sc_T profiles show an average magnitude of unity, as expected, at all measurement stations. For the polymer injection experiments, the Sc_T are all greater than unity with the highest magnitude measured

to be around 6. The magnitude increases with increasing concentration of the injected solutions. However, within each experiment, the estimated Sc_T decreases along the length of the flat plate showing loss of polymer effectiveness. The high Sc_T indicate that the turbulent mass flux away from the wall is affected by the action of the polymer such that the dispersion away from the wall is reduced. To achieve and maintain HDRs over a flat plate, the Sc_T needs to be high. This inhibits the flux of the polymer away from the wall and maintains the DR over a flat plate. The results presented here are among the first experimental measurements of the Sc_T in drag-reduced flows. It is hoped that this new experimental data will help in fine-tuning and benchmarking models used in computations of polymer DR.

This work is sponsored by Defense Advanced Research Projects Agency (DARPA), Advanced Technology Office, Friction Drag Reduction Program, DARPA Order No.: K042/31, K042/13, N115/00, issued by DARPA/CMO, Contract No. MDA972-01-C-0041. The content does not necessarily reflect the position or the policy of the U.S. Government, and no official endorsement should be inferred.

REFERENCES

Benzi, R., De Angelis, E., L'vov, V. S. & Procaccia, I. 2005 Identification and calculation of the universal asymptote for drag reduction by polymers in wall bounded turbulence. *Phys. Rev. Lett.* **95**, 194502.

Brungart, T. A., Harbison, W. L., Petrie, H. L. & Merkle, C. L. 1991 A fluorescence technique for measurement of slot injected fluid concentration profiles in a turbulent boundary layer. *Exp. Fluids* **11**, 9–16.

Elkins, C. J. 1997 Heat transfer in the rotating disk boundary layer. PhD thesis, Stanford University, Stanford, CA.

Fontaine, A. A., Petrie, H. L. & Brungart, T. A. 1992 Velocity profile statistics in a turbulent boundary layer with slot-injected polymer. *J. Fluid Mech.* **56**, 559–575.

Fruman, D. H. & Tulin, M. P. 1976 Diffusion of a tangential drag reducing polymer injection of a flat plate at high Reynolds numbers. *J. Ship Res.* **20**, 171–180.

Fukagata, K., Iwamoto, K. & Kasagi, N. 2002 Contribution of Reynolds stress distribution to the skin friction in wall-bounded flows. *Phys. Fluids* **14**, L73–L76.

Gupta, V. K., Sureshkumar, R. & Khomami, B. 2005 Passive scalar transport in polymer drag-reduced turbulent channel flow. *AIChE J.* **51** (7), 1938–1950.

Harder, K. J. & Tiederman, W. G. 1991 Drag reduction and turbulent structure in two-dimensional channel flows. *Phil. Trans. R. Soc. Lond.* A **336**, 19–34.

Hou, Y. X., Somandepalli, V. S. R. & Mungal, M. G. 2006 A technique to determine total shear stress and polymer stress profiles in drag reduced boundary layer flows. *Exp. Fluids* **40**, 589–600.

Hou, Y. X., Somandepalli, V. S. R. & Mungal, M. G. 2008 Streamwise development of turbulent boundary layer drag reduction with polymer injection. *J Fluid Mech.* **597**, 31–66.

Kawaguchi, Y., Segawa, T., Feng, Z. P. & Li, P. W. 2002 Experimental study on drag reducing channel flow with surfactant additives – spatial structure of turbulence investigated by PIV system. *Intl J. Heat Fluid Flow* **23**, 700–709.

Li, P., Kawaguchi, Y., Daisaka, H., Yabe, A., Hishida, K. & Maeda, M. 2001 Heat transfer enhancement to the drag-reducing flow of surfactant solution in two-dimensional channel with mesh-screen inserts at the inlet. *J. Heat Transfer* **123**, 779–789.

Li, F.-Ch., Kawaguchi, Y. & Hishida, K. 2003 Investigation on heat transfer characteristics of drag-reducing flow with surfactant additive by simultaneous measurements of temperature and velocity fluctuations in thermal boundary layer. In *Proceedings of the Sixth ASME/JSME Thermal Engineering Joint Conference*, Hawaii.

Luchik, T. S. & Tiederman, W. G. 1988 Turbulent structure in low-concentration drag-reducing channel flows. *J. Fluid Mech.* **190**, 241–263.

Lumley, J. L. 1969 Drag reduction by additives. *Annu. Rev. Fluid Mech.* **1**, 367–384.

L'vov, V. S., Pomyalov, A., Procaccia, I. & Tiberkevich, V. 2004 Drag reduction by polymers in wall bounded turbulence. *Phys. Rev. Lett.* **68**, 046308.

Petrie, H. L., Deutsch, S., Brungart, T. A. & Fontaine, A. A. 2003 Polymer drag reduction with surface roughness in flat-plate turbulent boundary layer flow. *Exp. Fluids* **35**, 8–23.

Petrie, H. L. & Fontaine, A. A. 1996 Comparison of turbulent boundary layer modification with slot-injected and homogeneous drag-reducing polymer solutions. *ASME Fluids Engng Div. Conf.* **237**, 205–210.

Procaccia, I., L'vov, V. S. & Benzi, R. 2008 Theory of drag reduction by polymers in wall-bounded turbulence, *Rev. of Modern Physics* **80** (1), 225–247.

Putorti, A. D., Jr, Everest, D. & Atreya, A. 2003 Simultaneous measurements of drop size and velocity in large-scale sprinkler flows using particle tracking and laser-induced fluorescence. *Tech Rep.* NIST GCR 03-852. National Institute of Standards and Technology.

Somandepalli, V. S. R. 2006 Combined PIV and PLIF measurements in a polymer drag reduced turbulent boundary layer. PhD thesis, Stanford University, Stanford CA.

Somandepalli, V. S. R., Hou, Y. X. & Mungal, M. G. 2005 Streamwise evolution of drag reduction in a boundary layer with polymer injection. In *Proceedings of Second Intl Symp. Sea Water Drag Reduction*, Busan, Korea.

Somandepalli, V. S. R., White, C. M. & Mungal, M. G. 2003 Boundary layer studies on polymer drag reduction using PIV and PLIF, ASME FEDSM 2003–45659. In *Proceedings of the ASME FEDSM 2003*, Hawaii.

Sreenivasan, K. R. & White, C. M. 2000 The onset of drag reduction by dilute polymer additives, and the maximum drag reduction asymptote. *J. Fluid Mech.* **409**, 149–164.

Tabor, M. & de Gennes, P. G. 1986 A cascade theory of drag reduction. *Europhys. Lett.* **2** (7), 519–522.

Toms, B. 1948 Observation on the flow of linear polymer solutions through straight tubes at large Reynolds numbers. *Proc. Intl Rheol. Congr.* **2**, 135–141.

Virk, P. S. 1975 Drag reduction fundamentals. *AIChE J.* **21**, 625–656.

Virk, P. S., Merril, E. W., Mickley, H. S., Smith, K. A. & Mollo-Christensen, E. 1967 The Toms phenomenon – turbulent pipe flow of dilute polymer solutions. *J. Fluid Mech.* **30**, 305–328.

Vdovin, A. V. & Smol'yakov, A. V. 1978 Diffusion of polymer solutions in a turbulent boundary layer. *Zh. Prikl. Mekh. Tekh. Fiz.* **2**, 66–73 (translation in UDC 532.526, pp. 196–201, Plenum).

Walker, D. T. & Tiederman, W. G. 1990 Turbulent structure in a channel flow with polymer injection at the wall. *J. Fluid Mech.* **218**, 377–403.

Warholic, M. D., Heist, D. K., Katcher, M. & Hanratty, T. J. 2001 A study with particle image velocimetry of the influence of drag reducing polymers on the structure of turbulence. *Exp. Fluids* **31**, 474–483.

Warholic, M. D., Massah, H. & Hanratty, T. J. 1999 Influence of drag-reducing polymers on turbulence: effects of Reynolds number, concentration and mixing. *Exp. Fluids* **27**, 461–472.

White, C. M. & Mungal, M. G. 2008 Mechanics and prediction of turbulent drag reduction with polymer additives. *Annu. Rev. Fluid Mech.* **40**, 235–256.

White, C. M., Somandepalli, V. S. R., Dubief, Y. & Mungal, M. G. 2006 Dynamic contributions to the skin friction drag in polymer drag reduced wall-bounded turbulence. *Phys. Fluids.* Manuscript submitted for publication.

White, C. M., Somandepalli, V. S. R. & Mungal, M. G. 2004 The turbulence structure of drag reduced boundary layer flow. *Exp. Fluids* **36**, 62–69.

Winkel, E. S., Oweis, G. F., Vanapalli, S. A., Dowling, D. R., Perlin, M., Solomon, M. J. & Ceccio, S. L. 2009 High Reynolds number turbulent boundary layer friction drag reduction from wall-injected polymer solutions. *J. Fluid Mech.* **621**, 259–288.

Wu, J. & Tulin, M. P. 1972 Drag reduction by ejecting additive solutions into a pure water boundary layer. *Trans. ASME D: J. Basic Engng* **94**, 749–755.

Yoshizawa, A. 2003 Turbulence-viscosity reduction mechanism based on anisotropic turbulence effects. *Phys. Fluids* **15**, 3875–3878.